NKS-488
ISBN 978-87-7893-584-7

Assessment of climate change's impacts on radioecological safety of subpolar and Nordic marine environment: Final Report from the NKS-B ANTHROPIC

Mu Lin[1], Jixin Qiao[1], Sven P. Nielsen[1], Gang Lin[1]
Yanchun He[2], Annette Samuelsen[2]
Emil Jeansson[3]
Kjartan Guðnason[4]
Karin Aquilonius[5], Pål Andersson[5], Anna Maria Blixt Buhr[5]
Vesa-Pekka Vartti[6], Pia Keski-Jaskari[6]

[1]Technical University of Denmark (Denmark)
[2]Nansen Environmental and Remote Sensing Center (Norway)
[3]Norwegian Research Centre (Norway)
[4]Icelandic Radiation Safety Authority (Iceland)
[5]Swedish Radiation Safety Authority (Sweden)
[6]Radiation and Nuclear Safety Authority (Finland)

October 2024

Abstract

This NKS-B ANTHROPIC project assesses climate-change impacts on radionuclide transport in Nordic and Arctic marine environments and associated radioecological risks using the Norwegian Earth System Model (NorESM).

NorESM was evaluated using historical data of reprocessing-derived radiotracers and chemical tracers, showing good performance, particularly in the Nordic Seas.

We simulated radionuclide transport from authorized discharges and a hypothetical nuclear accident under two different climate scenarios for 2015-2049. For authorized discharges, projections show largely steady-state transport along major pathways, with regional changes including increased flux into the Arctic Ocean via the Barents Sea and enhanced accumulation in the Beaufort Gyre. Few significant differences were observed between climate scenarios in the Nordic Seas. For hypothetical accident, the warmer climate showed lower long-term concentrations along the Norwegian coast, higher concentrations in central Nordic Seas, and lower concentrations in the Baltic Sea.

Risk assessments indicate that for authorized discharges, estimated doses remain well below public exposure limits with minimal climate-induced changes. For accidental releases, potentially significant impacts were identified in Danish, Swedish, and Norwegian waters, with cesium isotopes dominating dose contributions.

These findings suggest that current authorized discharge practices likely remain acceptable under near-term climate scenarios, but the long-term impacts on the radioecological risk and emergency preparedness needs to be investigated.

Key words

Radionuclide transport, Climate change, Nordic marine environment, Earth system model

NKS-488
ISBN 978-87-7893-584-7
Electronic report, October 2024

NKS Secretariat
P.O. Box 49
DK - 4000 Roskilde, Denmark
Phone +45 4677 4041
www.nks.org
e-mail nks@nks.org

Assessment of climate change's impacts on radioecological safety of subpolar and Nordic marine environment

Final Report from the NKS-B ANTHROPIC

(Contract: AFT/B(23)4)

Mu Lin[1], Jixin Qiao[1], Sven P. Nielsen[1], Gang Lin[1]
Yanchun He[2], Annette Samuelsen[2]
Emil Jeansson[3]
Kjartan Guðnason[4]
Karin Aquilonius[5], Pål Andersson[5], Anna Maria Blixt Buhr[5]
Vesa-Pekka Vartti[6], Pia Keski-Jaskari[6]

[1]Technical University of Denmark (Denmark)
[2]Nansen Environmental and Remote Sensing Center (Norway)
[3]Norwegian Research Centre (Norway)
[4]Icelandic Radiation Safety Authority (Iceland)
[5]Swedish Radiation Safety Authority (Sweden)
[6]Radiation and Nuclear Safety Authority (Finland)

Acknowledgements

The project partners of NKS-B ANTHROPIC appreciate the funding from NKS, the contributions from all participating organizations, and the support from other contributors in the Nordic research community. We are also deeply grateful to Xiaolin Hou, Elisabeth Tengborn, and Kasper Grann Andersson for their contributions to the project.

NKS conveys its gratitude to all organizations and persons who by means of financial support or contributions in kind have made the work presented in this report possible.

Disclaimer

The views expressed in this document remain the responsibility of the author(s) and do not necessarily reflect those of NKS. In particular, neither NKS nor any other organisation or body supporting NKS activities can be held responsible for the material presented in this report.

Table of contents

1. Introduction

1.1. NKS-B ANTHROPIC Project

For the sake of radioecological safety in the Nordic marine environment, great efforts have been dedicated to investigating the transport and bioaccumulation of radionuclides from well-documented sources (e.g., nuclear weapon testing, nuclear reprocessing plants, and the Chernobyl accident) (AMAP, 2016; HELCOM, 2018) or hypothetical accidents (e.g., the nuclear reactors and nuclear-powered vessels) (Reistad et al., 2012; Iosjpe et al., 2013; Nalbandyan et al., 2016; Anna Nalbandyan et al., 2017). However, due to the ongoing amplified ocean warming, sea-ice loss, and surface freshening in the Arctic Ocean and the Nordic Seas, the hydrology and circulation in the subpolar North Atlantic are subjected to fundamental changes (Masson-Delmotte et al., 2019), which may further trigger the changes in the dispersion modes of European coastal (radioactive) contaminations in the Nordic Seas. Hence, there is an urgent need to clarify whether and how climate change impacts the hydrodynamics and (radioactive) pollutant dynamics in the Nordic marine environment in the following decades.

The Earth system model (ESM) is a computational tool that integrate various components (atmosphere, oceans, land surface, and biosphere) of the Earth system and simulates the interactions (physical, chemical, and biological processes) between them to understand how different factors influence each other and predict climate variability and change. These models are essential for studying the effects of climate change, as they can project future environmental conditions based on different emission scenarios. In the context of radioecological research, ESMs can simulate the transport and fate of radionuclides in the marine environment, providing insights into how climate-induced changes in ocean circulation might alter the dispersion and accumulation of radioactive contaminants.

Utilizing the state-of-the-art Earth system model, the NKS-B ANTHROPIC project *"Assessment of climate change's impacts on radioecological safety of subpolar and Nordic marine environment"* seeks to project future transport and dispersion conditions (e.g., transport pathway, transit time, transfer factor, etc.) of radionuclides from authorized and accidental releases into the Nordic Seas under different climate-change scenarios and to assess the potential radioecological risks.

1.2. Norwegian Earth System Model (NorESM)

The Norwegian Earth System Model is the coupled Earth system model developed by the Norwegian Climate Center, which is based on the Community Earth System Model (CESM). The NorESM consists of several modules (**Figure 1**), including atmosphere, aerosol, ocean, biogeochemistry, sea ice, land, runoff, etc. Each module represents a specific component of the Earth's system and couples with others to simulate the complex interactions that drive the Earth's climate (Seland et al., 2020).

The NorESM can operate in either a fully-coupled configuration or a forced ocean-ice configuration. In the fully-coupled configuration, all NorESM's components are active and self-sustaining, enabling the simulation of historical states and future evolutions in different climate scenarios. The ocean-ice configuration of NorESM, in which only ocean and sea ice modules are active, is forced by the observation-based reanalysis data and can reproduce more realistic historical ocean currents but consume fewer computing and storage resources.

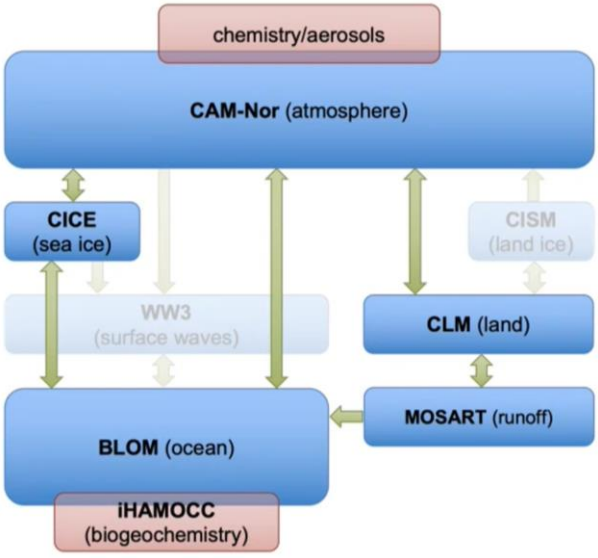

Figure 1. The model structure of NorESM (Seland et al., 2020).

1.3 Roadmap of NKS-B ANTHROPIC

The general roadmap of the NKS-B ANTHROPIC is illustrated in **Figure 2**. In short, the project began with a hindcast simulation (**WP1**) for the historical transport of the radioactive effluents from the European nuclear reprocessing plants at Sellafield and La Hague and the chemical tracers dissolved in the ocean surface. The hindcast simulation was performed in the ocean-ice configuration of NorESM, and the performance of the NorESM was evaluated by comparing the available observation datasets and obtained simulation results. As the performance of the NorESM was satisfactory, a projection simulation (**WP2**) was conducted in the fully-coupled configuration of NorESM for the dispersion of radionuclides from the authorized discharges from Sellafield and La Hague and accidental releases from a hypothetical nuclear accident in a warming climate. The climate-induced changes in the marine transport of radionuclides was analysed by comparing the historical periods and projection periods with two climate-warming scenarios. The potential dose contributions from fish consumption in climate-warming scenarios will be estimated and compared to assess the radioecological risks (**WP3**).

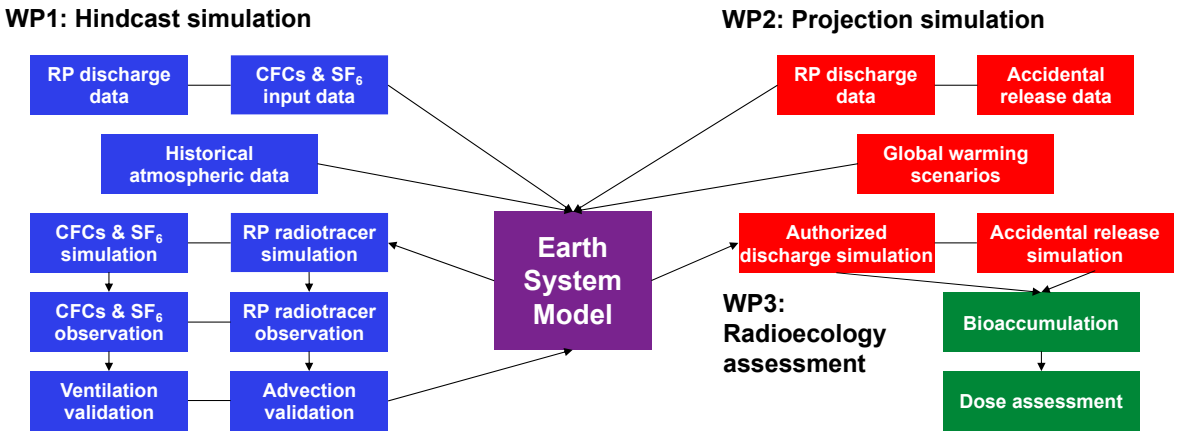

Figure 2. The general roadmap of NKS-B ANTHROPIC.

2. Evaluation of NorESM with hindcast simulation

2.1 Model setup for hindcast simulation

To evaluate the performance of NorESM in advection and ventilation transport of water masses, a hindcast simulations (1946-near present) was performed for the historical transport of radiotracers (^{99}Tc and ^{129}I) discharged from reprocessing plants and gaseous tracers (CFCs and SF_6) dissolved from the sea surface. Both reprocessing-derived radiotracers and chemical tracers have conservative behaviors and clear input history into the ocean (**Figure 3**), which can be used to trace the water-mass movement (Casacuberta and Smith, 2023). Their major difference is that the reprocessing-derived radiotracers are released from land-based point sources (European nuclear reprocessing plants at Sellafield and La Hague), mainly tracing the advection of the European coastal waters. Whereas the chemical tracers are fed into the ocean through the surface mixing layer, which mainly reveal the ventilation processes in the ocean.

^{99}Tc and ^{129}I are excellent radiotracers for evaluating the oceanic models. The liquid discharge from RPs is the dominating source of ^{99}Tc and ^{129}I in the environment (~93% and ~84%, respectively). Hence, the global-fallout-derived ^{99}Tc and ^{129}I could be ignored, enabling the direct comparison between the simulation results and observation datasets. In addition, ^{99}Tc and ^{129}I are traditionally regarded as conservative or near-conservative tracers in the open ocean (Casacuberta & Smith, 2023; M. Lin et al., 2023). The interactions of ^{99}Tc and ^{129}I with the particulate matters and organisms are presumed minimal, obviating the need for considering specific geochemical or biological processes in the simulation.

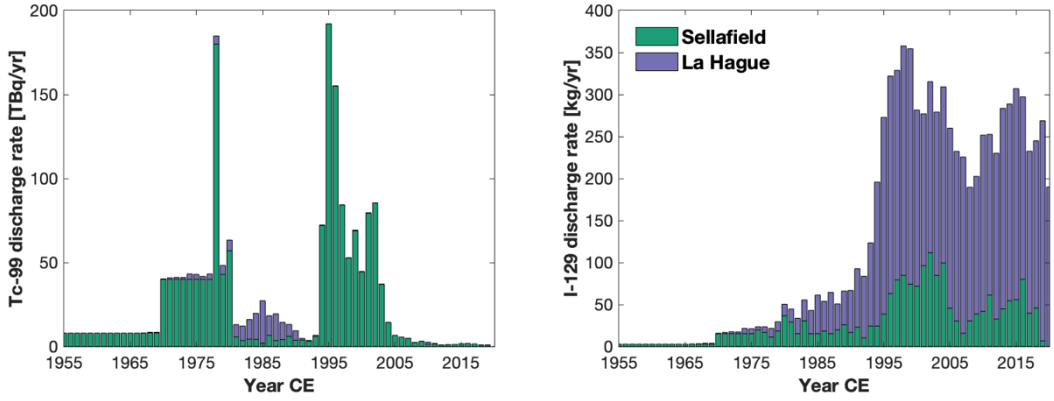

Figure 3. The discharge history of Tc-99 and I-129 from the two European nuclear reprocessing plants at Sellafield and La Hague (European Commission, 2022; HELCOM, 2020).

The hindcast simulations was conducted in both ocean-ice configuration and fully-coupled configuration (see the detailed model setup in **Table 1**). Afterwards, the spatiotemporal distribution of radiotracers and chemical tracers simulated by the NorESM was compared against their observations. The observation datasets of radiotracers consist of 2238 records for Tc-99 and 852 records for I-129, which are compiled from the published and internally archived spatial-distribution and time-series observation results of radiotracers in the North Atlantic and Arctic Oceans during the 1960s-2010s (Casacuberta et al., 2018, 2016; Castrillejo et al., 2018; Christl et al., 2015; Gómez-Guzmán et al., 2014, 2013; He et al., 2022; Hou et al., 2007, 2000; IAEA, 2023; Lin et al., 2022; Nagai et al., 2019; Nies et al., 2008; Qiao et al., 2021, 2020; Smith et al., 2021; Vivo-Vilches et al., 2018; Wefing et al., 2019). The basin-wide cross sections of CFCs' observations in the North Atlantic can be obtained from the World Ocean Circulation Experiment (WOCE) and following observational campaigns (https://cchdo.ucsd.edu/).

Table 1. The model setup of NorESM for hindcast simulation.

Hindcast simulation	**Study Case 1: reprocessing-derived radiotracers**	**Study Case 2: chemical tracer**
Purpose	Validate NorESM and study the advection dynamic processes	Validate NorESM and study the ventilation dynamic processes
Tracer	Tc-99 ($T_{1/2}$ = 0.211 Myr.) and I-129 ($T_{1/2}$ = 15.7 Myr.)	CFC-11, CFC-12, and SF_6
Time period	1945-2023 (ocean-ice configuration) and 1945-2019 (fully-coupled configuration)	
Source term	Sellafield and La Hague	Sea surface
Input function	Tc-99 and I-129: HELCOM and RADD discharge database (European Commission, 2022; HELCOM, 2020)	CFCs and SF_6: time-series concentrations in atmosphere (Bullister, 2015)
Model configuration	Ocean-ice configuration and fully-coupled configuration	
Atmospheric forcing for ocean-ice configuration	The Japanese 55-year Atmospheric Reanalysis datasets (Kobayashi et al., 2015)	

2.2 Performance of NorESM

2.2.1 Advection transport

2.2.1.1 Evaluation with spatial-distribution observations

The spatiotemporal distribution of the reprocessing-derived Tc-99 and I-129 in the surface waters of the North Atlantic and Arctic Oceans, as simulated by the NorESM in the ocean-ice configuration, is shown in **Figures 4 and 5**, respectively. It should be noted that the unit of I-129 concentration is atoms/kg instead of Bq/kg that is commonly used for other radionuclides. This is because the concentration of long-lived I-129 is quite low in seawater and usually measured by the accelerator mass spectrometry.

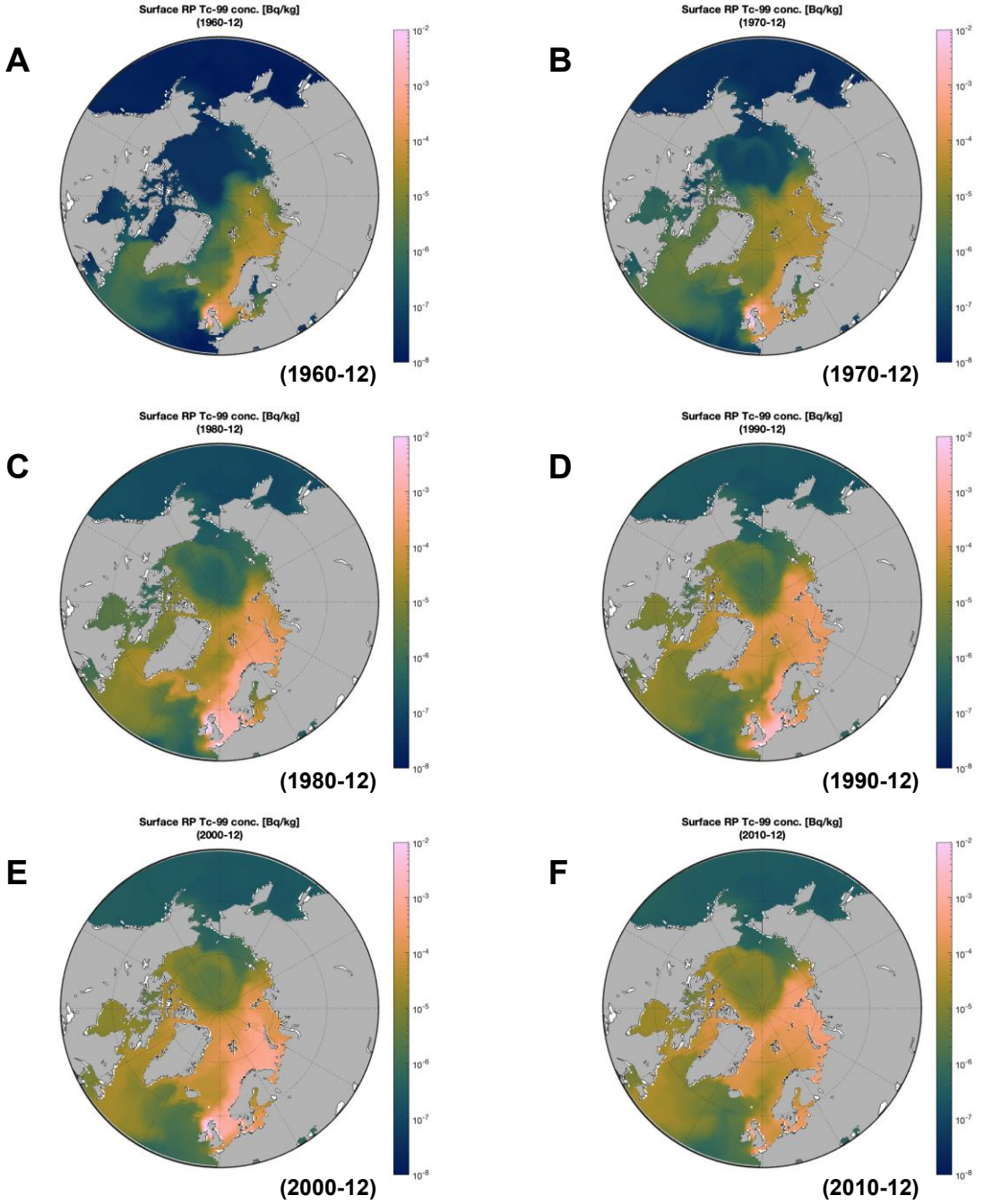

Figure 4. The distribution of Tc-99 (Bq/kg) released from Sellafield and La Hague in the surface water of the North Atlantic and Arctic Oceans simulated by the NorESM in the ocean-ice configuration.

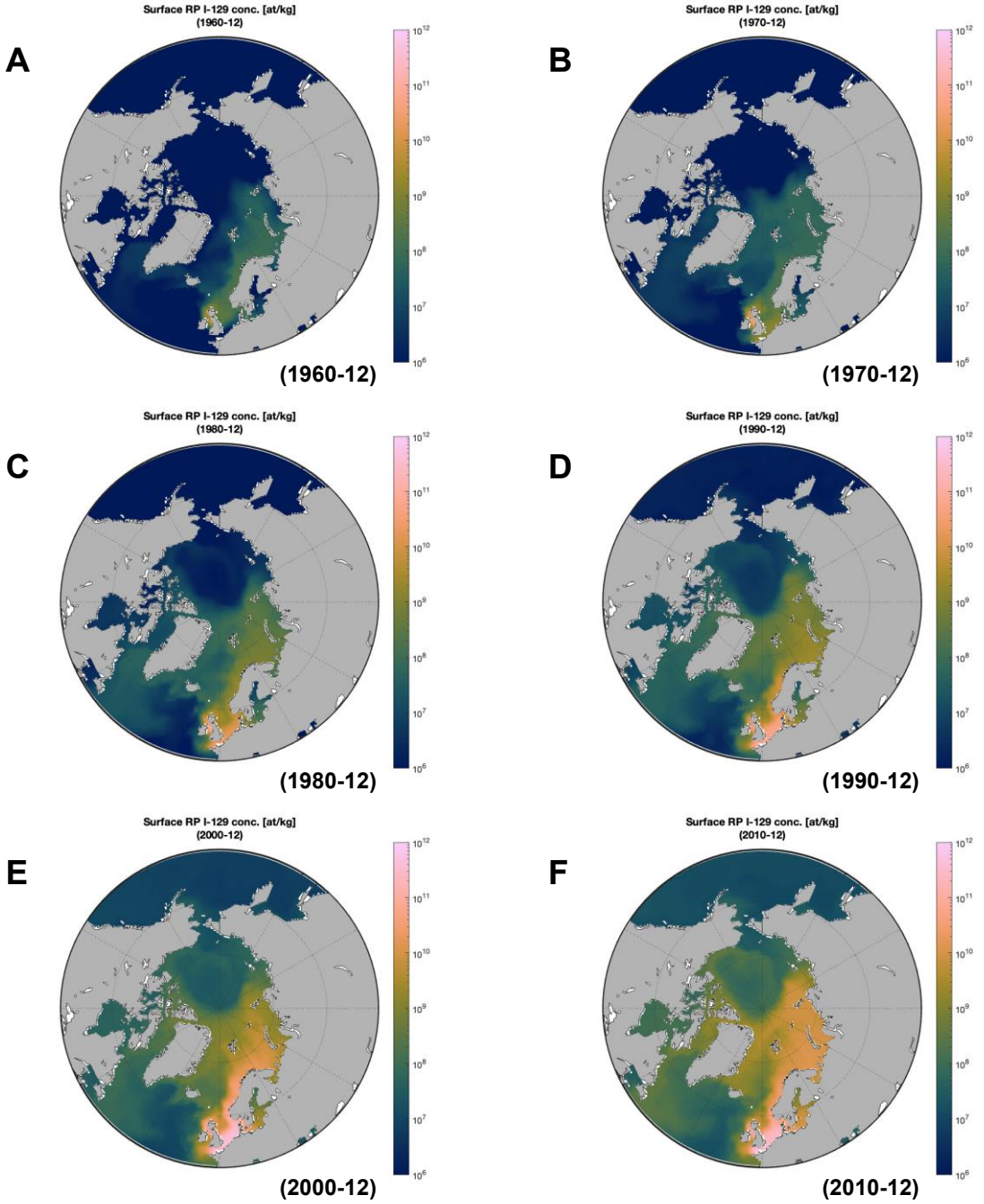

Figure 5. The distribution of I-129 (atoms/kg) released from Sellafield and La Hague in the surface water of the North Atlantic and Arctic Oceans simulated by the NorESM in the ocean-ice configuration.

The comparison between the observations of Tc-99 and I-129 in the North Atlantic and Arctic Oceans and corresponding simulations by NorESM in the ocean-ice configuration is shown in **Figures 6** and summarized in **Table 2**. In general, the ocean-ice configuration of NorESM shows an overall good performance in reproducing the advection transport in the North Atlantic and Arctic Oceans. **For the Nordic Seas where we have more interests, the NorESM has better performance than the other regions.**

For Tc-99, the simulated concentrations agree well with the observations in the Nordic Seas (mean relative bias: 3.4%; correlation coefficient: 0.812) and Arctic Ocean (mean relative bias: 43.3%; correlation coefficient: 0.906). However, larger discrepancies are found in the Baltic Sea (mean relative bias: 63.2%; correlation coefficient: 0.427) and North Atlantic (mean relative bias: 39.1%; correlation coefficient: 0.292). The overall mean relative bias and correlation coefficient between simulations and observations are 33.8% and 0.427 for the entire study area, respectively.

For I-129, the model performance is generally better than that for Tc-99. Strong agreement is achieved in the North Atlantic (mean relative bias: 73.6%; correlation coefficient: 0.830) and Nordic Seas (mean relative bias: 23.9%; correlation coefficient: 0.830). Moderate correlation is found in the Baltic Sea (mean relative bias: 45.3%; correlation coefficient: 0.531) and Arctic Ocean (mean relative bias: -38.8%; correlation coefficient: 0.529). The overall mean relative bias and correlation coefficient reach 11.2% and 0.795 for the entire study area.

The large discrepancies between simulated and observed I-129 concentrations in the Arctic Ocean, particularly in the bottom of the Beaufort Gyre (**Figure 6, C and D**), suggest that NorESM has a poor performance in reproducing the circulation and ventilation processes in this area. The underestimation of I-129 concentrations in the Beaufort Gyre could be attributed to two possible reasons: 1) the model's inability to accurately simulate the advection of I-129 from the North Atlantic into the Arctic Ocean, resulting in less or slower transport of I-129 to the Beaufort Gyre; and 2) the model's inadequacy in reproducing the ventilation processes within the Beaufort Gyre, leading to an underestimation of the mixing between surface and deep waters. The relatively poor performance in the Baltic Sea (North-Baltic Sea Transition Zone) for both radiotracers can be attributed to the model's coarse resolution in representing the complex topography and circulation in the semi-closed regions.

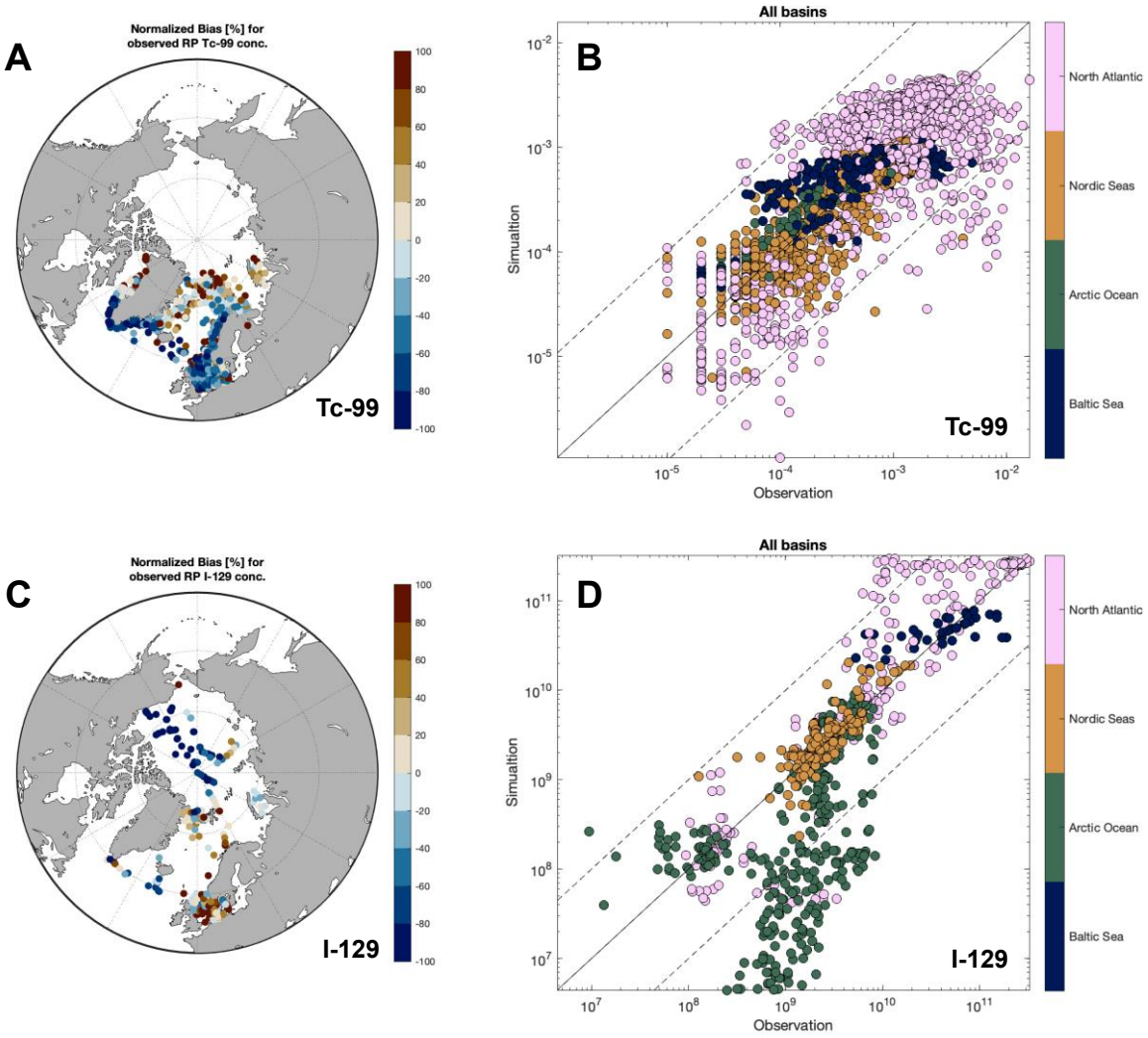

Figure 6. The spatial distribution of observations of Tc-99 (A) and I-129 (C) in the North Atlantic and Arctic Oceans, and the comparison between the observations and corresponding simulations for Tc-99 (B) and I-129 (D) in the **ocean-ice configuration**. In plot A and C, the normalized bias is the difference between simulated and observed values divided by the observed value; for plot B and D, the comparison results are summarized in **Table 2**.

Table 2. Evaluation of NorESM's performance in advective transport by comparing the observation datasets with the simulation results of reprocessing-derived Tc-99 and I-129 in the North Atlantic and Arctic Oceans. The bias is calculated by the difference between the mean of the predicted values by NorESM and the mean of observed values; the relative bias is the ratio of the bias and the mean of observed values. The correlation coefficient is calculated by the Pearson product-moment correlation analysis, and its significance has been tested with the two-tail test at a confidence level of 95%.

Observation vs. simulation: Tc-99			**Observation vs. simulation: I-129**		
Region	**Relative bias**	**Correlation coefficient**	**Region**	**Relative bias**	**Correlation coefficient**
Ocean-ice configuration					
Baltic Sea (n=480)	63.2%	0.427	Baltic Sea (n=92)	45.3%	0.531
Arctic Ocean (n=134, outliers excluded)	43.3%	0.906	Arctic Ocean (n=323, outliers excluded)	-38.8%	0.529
Nordic Seas (n=612)	3.4%	0.812	Nordic Seas (n=179)	23.9%	0.830
North Atlantic (n=1011, outliers excluded)	39.1%	0.292	North Atlantic (n=225, outliers excluded)	73.6%	0.830
Overall (n=2238)	**33.8%**	**0.427**	**Overall (n=852)**	**11.2%**	**0.795**
Fully-coupled configuration					
Baltic Sea (n=480)	36.1%	0.234	Baltic Sea (n=92)	40.0%	0.720
Arctic Ocean (n=134, outliers excluded)	22.3%	0.798	Arctic Ocean (n=323, outliers excluded)	-61.8%	0.544
Nordic Seas (n=612)	-13.5%	0.766	Nordic Seas (n=179)	48.4%	0.376
North Atlantic (n=1011, outliers excluded)	32.0%	0.199	North Atlantic (n=225, outliers excluded)	76.0%	0.793
Overall (n=2238)	**19.3%**	**0.334**	**Overall (n=852)**	**6.82%**	**0.817**

2.2.1.2 Evaluation with time-series observations

Besides spatial-distribution observations, eight time-series observation datasets obtained at six coastal stations in the North Atlantic and Nordic Seas were also used to evaluate the NorESM's performance in reproducing the advective transport of radiotracers along the coastal currents, which is shown in **Figure 7** and summarized in **Table 3**.

The comparison of simulation results with time-series observations at coastal stations reveals that the ocean-ice configuration of NorESM has a satisfactory performance in reproducing the temporal evolution of reprocessing-derived radiotracers in coastal areas. For eight time-series observation datasets, the mean relative biases varying from -38.3% to 39.7%, which is acceptable considering that the measurement uncertainties are normally between 10% and 30%.

For Tc-99, the relatively poor performance at some coastal stations, particularly in the Danish Straits and along the Norwegian coast, may result from the model's limited ability to resolve the complex coastal circulation patterns and the influence of local-scale processes, such as freshwater inputs and tidal mixing. At the stations Klint and Utsira, the NorESM has better performance in simulating I-129/I-127 ratios compared to Tc-99 concentrations, which can be attributed to the fact that the former is less sensitive to the variabilities in salinity. Both stations are located at the transition region between the North Sea and Baltic Sea, which receives large freshwater inputs from the Baltic outflowing water.

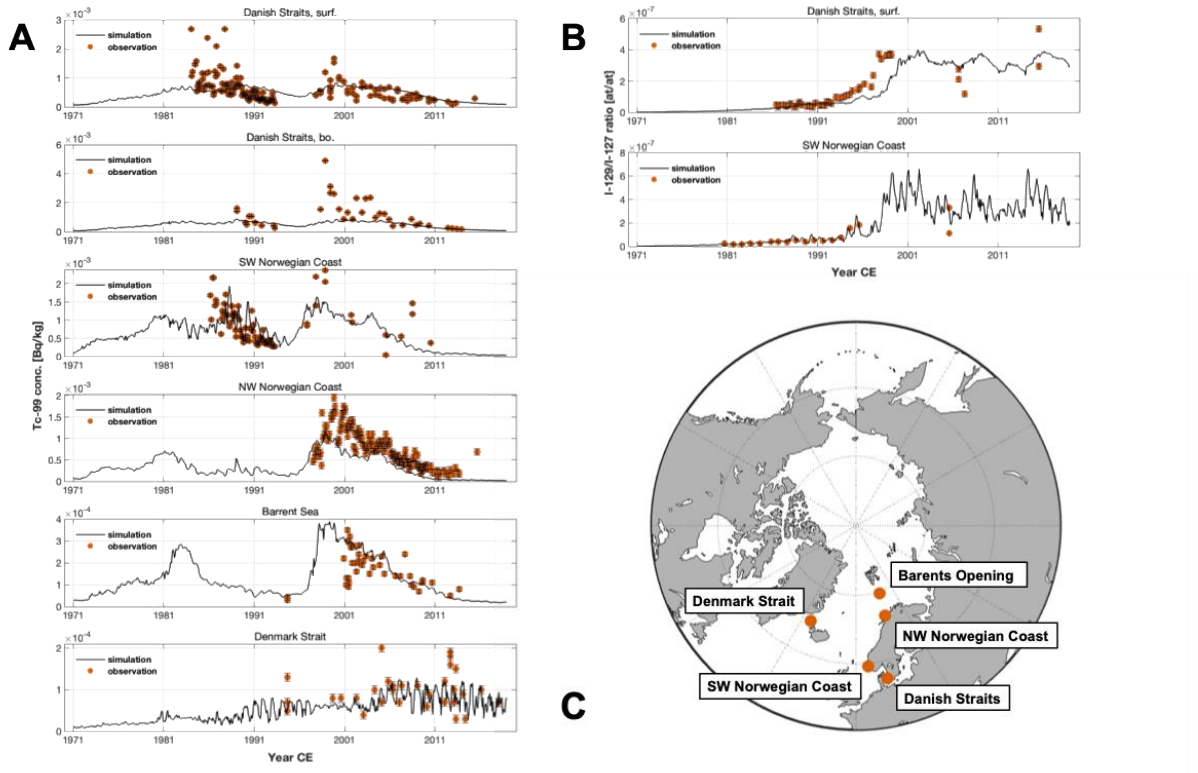

Figure 7. The comparison between simulation results (ocean-ice configuration) and time-series observations for Tc-99 (A) and I-129 (B) at various coastal sites (C). The comparison results are summarized in **Table 3**.

Table 3. Summary for the comparison between simulation results and time-series observations. The bias is calculated by the difference between the mean of the predicted values by NorESM and the mean of observed values; the relative bias is the ratio of the bias and the mean of observed values. The correlation coefficient is calculated by the Pearson product-moment correlation analysis, and its significance has been tested with the two-tail test at a confidence level of 95%.

No.	Tracer	Sample type	Sample number	Location	Relative bias	Correlation coefficient
1	^{99}Tc conc.	surface seawater	164	Klint, Denmark (55.97°N, 11.58°E)	39.7%	0.166
2	^{99}Tc conc.	bottom seawater	37	Klint, Denmark (55.97°N, 11.58°E)	-19.2%	0.428
3	^{99}Tc conc.	surface seawater	81	Utsira, Norway (59.18°N, 4.53°E)	28.9%	0.418
4	^{99}Tc conc.	surface seawater	159	Hillesøy, Norway (69.62°N, 17.95°E)	-38.3%	0.753
5	^{99}Tc conc.	surface seawater	42	Bjørnøya, Norway (74.54°N, 19.09°E)	35.8%	0.681
6	^{99}Tc conc.	surface seawater	33	Denmark Strait (67.25°N, 25.58°W)	-11.3%	not corr.
7	^{129}I/^{127}I ratio	seaweed	46	Klint, Denmark (55.97°N, 11.58°E)	-23.2%	0.753
8	^{129}I/^{127}I ratio	seaweed	19	Utsira, Norway (59.18°N, 4.53°E)	-12.9%	0.923

2.2.1.3 Difference between ocean-ice and fully-coupled configurations

As the projection simulation would be performed in the fully-coupled configuration, it's necessary to evaluate the performance of the fully-coupled configuration as well. The comparison results between observations and simulations in the fully-coupled configuration are shown in **Figures 8** and summarized in **Table 2**.

In general, the fully-coupled configuration shows comparable overall performance with the ocean-ice configuration. For Tc-99, even though the correlation coefficient for the entire study area decreases from 0.427 (ocean-ice) to 0.334 (fully-coupled), the mean relative bias improves from 33.8% (ocean-ice) to 19.3% (fully-coupled). For I-129, the overall correlation coefficient increases from 0.795 (ocean-ice) to 0.817 (fully-coupled), and the mean relative bias drops slightly from 11.2% (ocean-ice) to 6.82% (fully-coupled).

While in the Nordic Seas where we have more interests, the fully-coupled configuration, with only green-house gasses and radiative forcings, has slightly worse performance than the ocean-ice configuration, with more constraints by the observation-based air-sea flux from the atmospheric reanalysis datasets. It is therefore expected that the coupled system has better internal dynamical consistent but may have larger deviation compared to observation. The NorESM also has even worse performance in the bottom of the Beaufort Gyre region in the fully-coupled configuration, as revealed larger discrepancies between simulated and observed I-129 concentrations. It suggests that the resolved and parameterized processes may need to be further improved in the ocean component of NorESM, particularly in this central Arctic region.

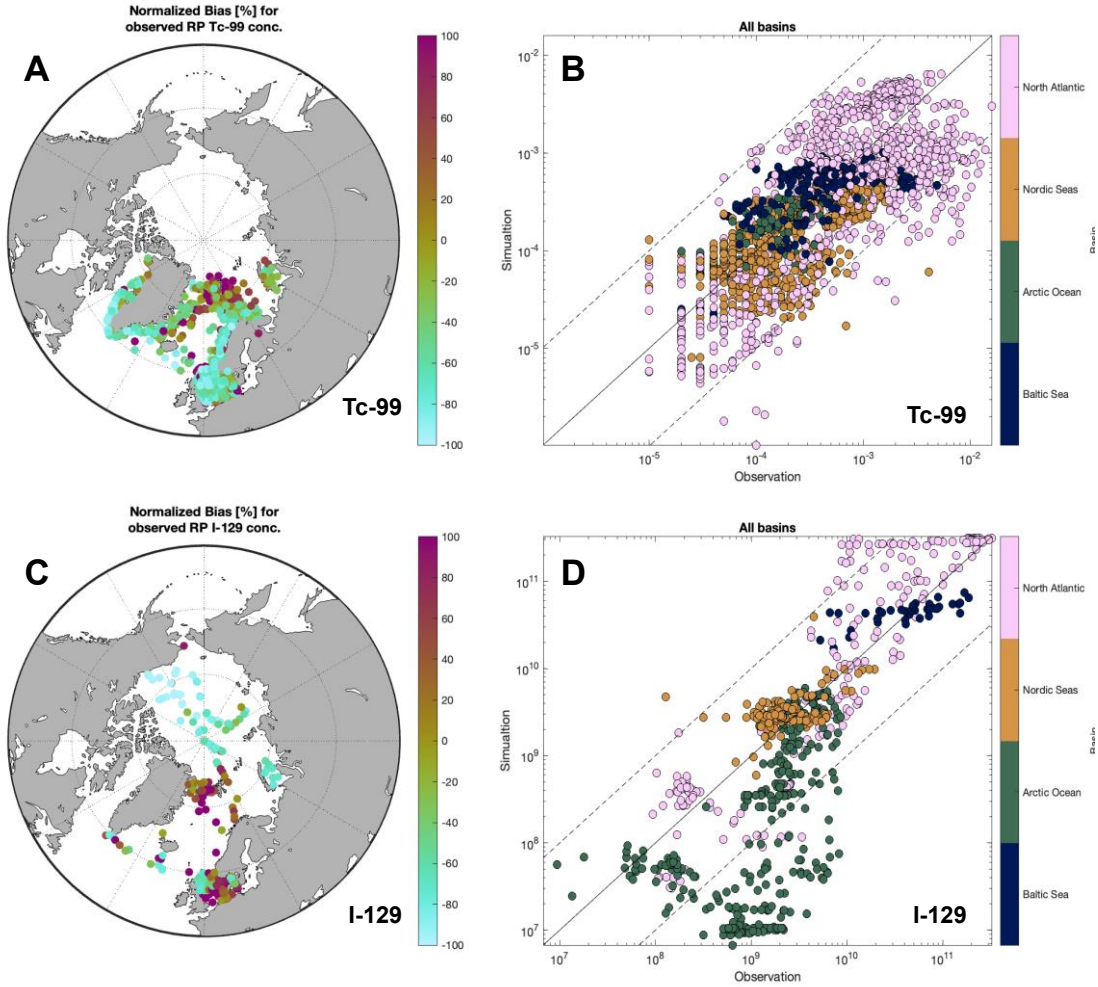

Figure 8. The spatial distribution of observations of Tc-99 (A) and I-129 (C) in the North Atlantic and Arctic Oceans, and the comparison between the observations and corresponding simulations for Tc-99 (B) and I-129 (D) in **fully-coupled configuration**. In plot A and C, the normalized bias is the difference between simulated and observed values divided by the observed value; for plot B and D, the comparison results are summarized in **Table 2**.

2.2.2 Ventilation transport revealed by chemical tracers

The chemical tracers, including chlorofluorocarbons (CFCs) and sulphur hexafluoride (SF_6) are included between 1910 and 2015 in the carbon cycle component (HAMOCC) of the NorESM. Observations of these passive tracers are available since the 1980s and are synthesized through the GLODAP project (Lauvset et al., 2021). The simulated hydrology (temperature, salinity), passive tracers (CFC-12 and SF_6), and biogeochemical tracer (oxygen) are compared with the GLODAPv2.2023 datasets to get a quick evaluation of the model performance in the ventilation processes in the Nordic Seas and Arctic Ocean. Three cross sections are selected for the comparisons. These sections are along the transport pathway of Atlantic water from the subpolar to the Arctic Ocean, including the Norwegian coast section (Cruise ID: 58GS20150410), the Fram Strait (Cruise ID: 06AQ20120614), and the central Arctic Ocean section (Cruise ID: 33HQ20150809).

In the section along the Norwegian coast (**Figure 9**), the fingerprint of warm and saline Atlantic Water in the observation is remarkable west of 3.5ºE, and the cold and fresh coastal water dominate the upper 50 m east of 3.5ºE. The oxygen is featured with a high concentration above 320 µmol/kg shallow layer (0-20 m) and a thick subsurface layer of deficient oxygen (lower than 280 µmol/kg). The model simulation reproduces these observed features well, demonstrating the model's ability to represent the Atlantic Water and the Norwegian coast circulation given its limitation of coarse resolution. However, the observed and simulated CFC-12 and SF_6 differ substantially with each other. The simulated CFC-12/SF_6 have a strong signal of subsurface coastal water, and further examination showing that the source of the subsurface maximum comes from the region of Skagerrak Strait (not shown as figure). The observed distribution of CFC-12/SF_6 are however much patchy and differ substantially with the simulated distribution. Though the model simulated hydrology and ventilation in general agree with the observation, the simulated transient evolution of CFC-12 and SF_6 tracers are controlled by many different factors, including the hydrology, circulation and parameterised air-sea fluxes. **Given those limitations, the model has difficulties in reproducing the transient statues of the observed CFC-12/ SF_6 in this section close to the coast with complex circulations.**

In the section of Fram Strait (**Figure 10**) the cold and fresh Arctic surface water is presented in the shallow layer in the Greenland continental shelf west of 5ºW, and the warm and saline Atlantic Water occupies the subsurface layer (0-400 m) in the eastern part of the Fram Strait. This distinction of the Arctic Water and Atlantic Water is also visible in the observed CFC-12 and SF_6 data. **The model simulation well represents the observed distribution of temperature, salinity, CFC-12 and SF_6 in the Norwegian coast, which are consistent with the better performance in the Nordic Seas revealed by radiotracers.**

In the section from the Canadian Basin to the Central Arctic (**Figure 11**), both the observation and the simulation are close with respect to the hydrology. They also have high concentration of CFC-12/SF6 tracers in the upper layer, but the tracers are more concentrated in the surface layer in the simulation, while the observed tracers are mixed into much deeper depth. **Even though the spreading of high CFC-12/SF6 are somehow constrained by the Alpha Ridge, the weaker vertical mixing processes in the NorESM may have more impacts on the less simulated CFC-12/SF_6, as well as the radiotracers, in the deeper layers of the Canadian Basin.**

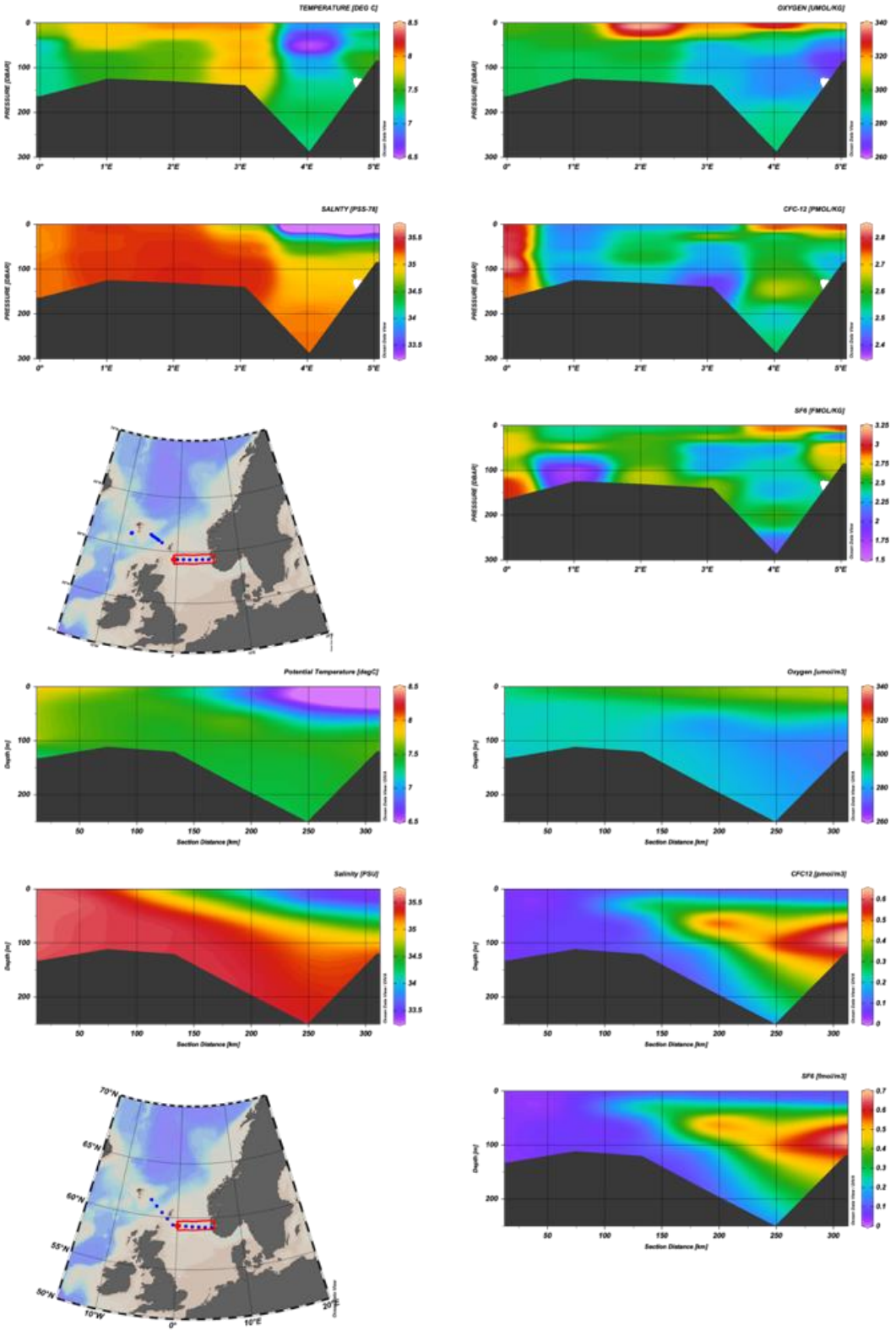

Figure 9. Observed (upper, GLODAPv2.2023) and simulated (lower, NorESM) temperature, salinity, CFC-12, SF_6 and oxygen across section from Faroe Island to Norwegian coast at 60ºN (Cruise ID: 58GS20150410). Also note the color scale of the simulated CFC-12/SF_6 is about 4 times smaller than the observation.

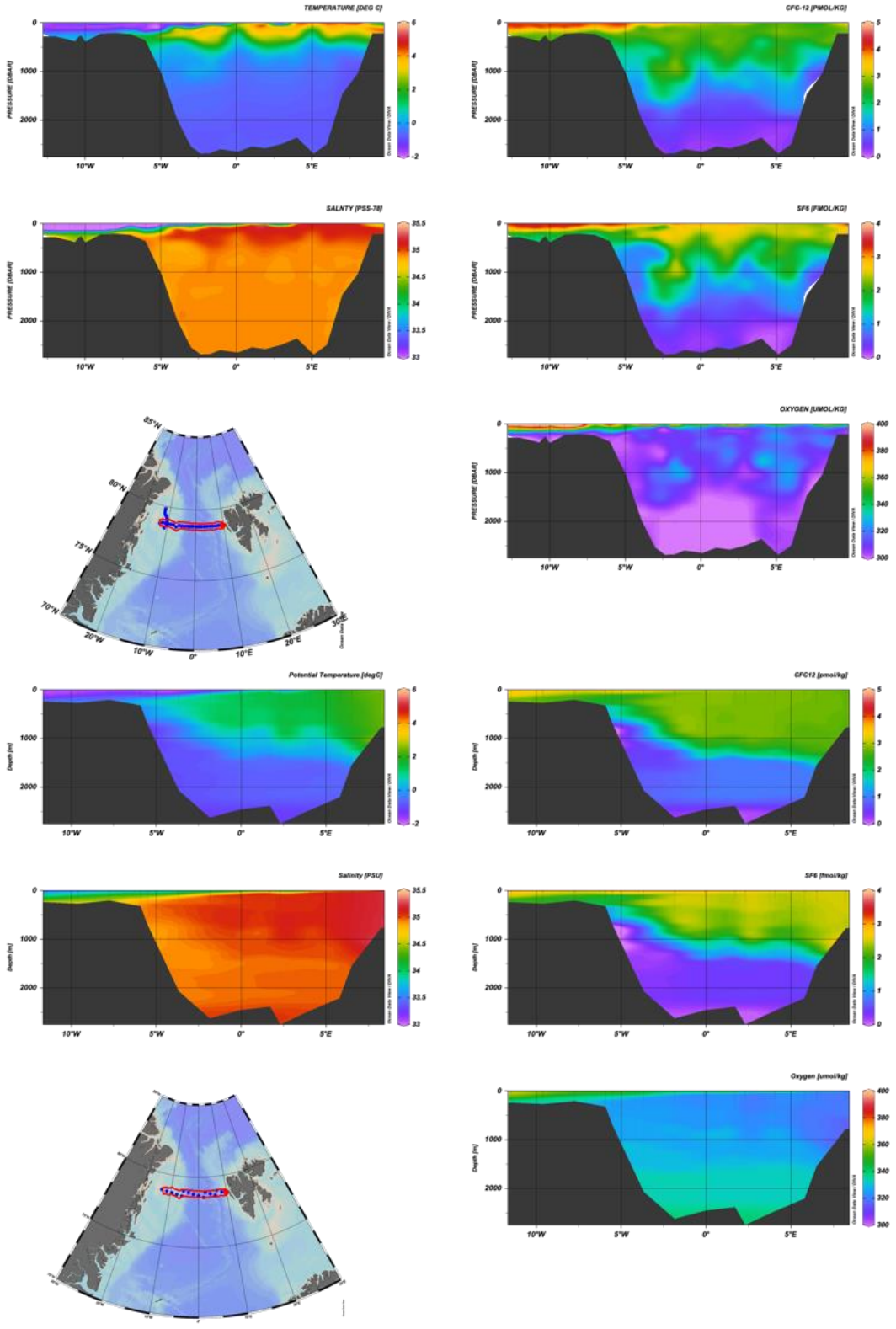

Figure 10. The same as **Figure 9** but for the section across the Fram Strait (Cruise ID: 06AQ20120614)

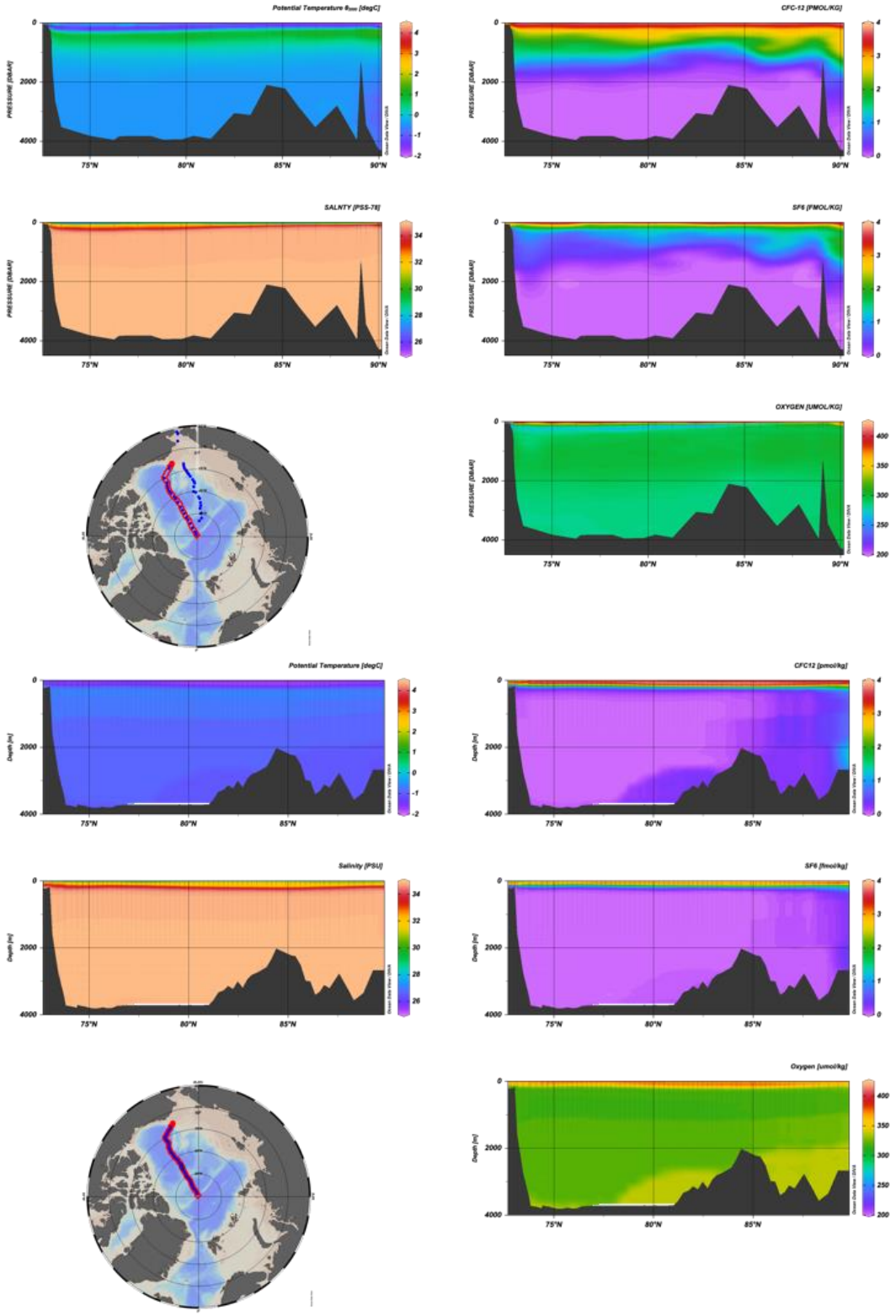

Figure 11. The same as **Figure 9** but for the section in the Central Arctic from the Canadian Basin to the North Pole (Cruise ID: 33HQ20150809e).

2.3 Summary

The hindcast simulation using NorESM demonstrated its capability to reproduce the historical transport of radiotracers in the North Atlantic and Arctic Oceans. The model showed good performance in simulating the advection of radiotracers, as well as the ventilation of chemical tracers, particularly in the Nordic Seas. The model successfully captured the major transport pathways of radiotracers, including northward transport along the Norwegian coast, entry into the Arctic Ocean via the Barents Sea and Fram Strait, circulation within the Arctic, and southward transport along the East Greenland Current. The simulation also accurately represented the timescales of transport, with transit times increasing from a few years near the source to over 20 years in the Arctic and North Atlantic. While some discrepancies were observed, particularly in semi-enclosed basins like the Baltic Sea and central Arctic Ocean, the overall performance of NorESM in reproducing radiotracer transport supports its use for projecting future scenarios under different climate conditions.

3. Projection of future radioactive pollutant dynamics

3.1 Model setup for projection simulation

As NorESM shows satisfactory performance in advection and ventilation transport of water masses, a forecast simulation (2015-2049) was performed to predict the future radioactive pollutant dynamics in the Nordic Seas and Arctic Ocean. Two cases were considered in the forecast simulation:

- authorized discharges from the two nuclear reprocessing and waste treatment facilities at Sellafield (the reprocessing has stopped but the discharges from waste treatment will continue) and La Hague during 2015-2060 (**Study Case 3**).
- accidental releases from a hypothetical nuclear accident in the Swedish nuclear power plant Ringhals in 2040 (**Study Case 4**).

Table 4. The model setup of NorESM for projection simulation.

Projection simulation	**Study case 3: authorized discharges from reprocessing plants**	**Study case 4: accidental releases from a nuclear accident**
Tracer	I-129 ($T_{1/2}$ = 15.7 Myr.) Cs-137 ($T_{1/2}$ = 30.1 yr)	I-129 ($T_{1/2}$ = 15.7 Myr.) Cs-137 ($T_{1/2}$ = 30.1 yr) Sr-90 ($T_{1/2}$ = 28.8 yr) Cs-134 ($T_{1/2}$ = 2.07 yr) I-131 ($T_{1/2}$ = 8.02 d)
Time period	2015-2049	2040-2049
Source term	Sellafield and La Hague	Unit 4, Ringhals Nuclear Power Plant
Input function	Constant discharge: I-129: 200 kg/yr. (9.33×10^{27} atoms/yr.) Cs-137: 1.00 TBq/yr.	Pulse release for both direct discharge and atmospheric deposition (field source) *
Model configuration	Fully-coupled configuration	
Climate-warming scenarios	Middle (SSP245) and high (SSP585) emissions	

* In principle, the deposition pattern highly depends on the weather conditions when the accident happens and varies case by case. However, to make a better comparison, we use the same deposition pattern for the projections with different climate-warming scenarios.

In the case of authorized discharges from the reprocessing plants, I-129 and Cs-137 were selected as the targeted radionuclides. Their relatively long half-lives, conservative behaviours, and higher bioaccumulation tendency contribute to their long-distance transport and high contribution to the human doses (Nielsen et al., 1995). A constant discharge rate was assumed for the discharge of each radionuclide during the simulation period. The transport pathway and timescale of reprocessing-derived radionuclides were investigated based on the distribution and trend of the flux strength, mean transit time, and mean flux depth. The dilution of reprocessing-derived radionuclides in the surface waters was represented by the transfer factor.

In the case of accidental releases from a hypothetical nuclear accident, a Fukushima-type nuclear accident was assumed to occur in the Unit 4 of Ringhals Nuclear Power Plant (R4). The source term and deposition pattern on the adjacent sea surface were provided by SSM with the

support from the Swedish Meteorological and Hydrological Institute (SMHI) and based on previous work (Sergey Galushin et al., 2022). The subsequent oceanic transport of I-129, Cs-137, Sr-90, Cs-134, and I-131 from was simulated by NorESM.

For both two cases, the projection simulations were conducted in the fully-coupled configuration of NorESM with two climate projection scenarios corresponding to different emission scenarios, the so-called Shared Socioeconomic Pathways (including SSP245 and SSP585) (Gidden et al., 2019).

3.2 Climate-induced Changes in Radioactive Pollutant Transport

3.2.1 Authorized discharges from the reprocessing plants

3.2.1.1 Transport pathway and timescale

Figure 12 presents the mean transport pathway and associate timescale of radioactive pollutants from the European reprocessing plants (here we only present the results for LH-derived I-129 as representative). The La-Hague-derived (LH-derived) radionuclides are initially transported northwards along the western coast of Europe by the European Coastal Current, as indicated by the high flux values and shallow mean depth in this region (**Figure 12A** and **G**). The mean transit time in this region is relatively short, less than 5 years (**Figure 12D**). As the LH-derived radioactive pollutants reach the North Sea, it is partially carried into the interior Baltic Sea by the Baltic Inflowing Water, while the majority continues flowing northwards along the Norwegian coast via the Norwegian Coastal Current. The transit time in the North Sea and along the Norwegian coast is around 5-10 years, with the LH-derived radionuclides confined mainly to the upper layers (< 500 m). Upon reaching the Nordic Seas, the LH-derived radionuclides are carried into the Barents Sea and the Arctic Ocean by the North Cape Current, as well as into the deep basins of the Nordic Seas. The transit time in the Nordic Seas is approximately 10-15 years, with the LH-derived radionuclides found at depths ranging from the surface to over 1000 m.

In the Arctic Ocean, the LH-derived radionuclides are transported across the basin by the Transpolar Drift Stream, with a portion flowing into the Canadian Basin. The transit time in the central Arctic Ocean is around 15-20 years, and the mean depth of the LH-derived radionuclides exceeds 1000 m due to deep convection and mixing processes. The LH-derived radionuclides exit the Arctic Ocean through two main pathways: the Canadian Archipelago and Fram Strait. The LH-derived radionuclides passing through the Canadian Archipelago has a longer transit time (> 20 years) and is confined to shallower depths (< 500 m) compared to the LH-derived radionuclides exiting via Fram Strait, which has a transit time of 15-20 years and a mean depth of 500-1000 m.

After exiting the Arctic Ocean, the LH-derived radionuclides is exported to Greenland Sea through the Fram Strait and eventually to the Central Larador sea through as the Denmark Strait Overflow Water (DSOW). The transit time in the Greenland and Labrador Seas is around 15-20 years, with the LH-derived radionuclides found at depths of 500-1000 m. The LH-derived radionuclides in the Nordic Seas are also transported to the North Atlantic Ocean through the Faroe Bank Channel Overflow (FBCO). The LH-derived radionuclides passing through the FBCO have a longer transit time (> 20 years) and a deeper mean depth (> 1000 m) compared to the LH-derived radionuclides transported by the DSOW.

Finally, the LH-derived radionuclides transported into the North Atlantic Ocean are gradually mixed into the subpolar gyre. The transit time in the North Atlantic exceeds 20 years, and the mean depth of the LH-derived radionuclides is greater than 1000 m due to deep mixing processes.

Figure 13 presents the trend slope for the depth-integrated flux of LH-derived I-129, the corresponding mean transit time, and mean depth of I-129 flux during 1980-2049. In general, both scenarios present **a steady-state transport (flux strength, transit time, and depth) of reprocessing-derived radionuclides along the major transport pathway entering and exiting the Arctic Ocean: the European Coastal Current, Norwegian Coast Current, Norwegian Coast Current and its extension, Transpolar Drift Stream, and East Greenland Current.** The only exception is the branch entering the Arctic Ocean via the Fram Strait, which shows a decrease trend in flux strength and an increase trend in transit time, indicating that **reprocessing-derived radionuclides tend to enter the Arctic Ocean via the Barents Opening under warmer conditions**.

However, different changes can be observed in the coastal regions of Barents and Kara Seas, the Beaufort Gyre, and the central Nordic Seas:

- In the coastal regions of the Barents and Kara Seas, both scenarios show an increasing trend in flux strength with unchangeable transit time and depth support the conclusion that more reprocessing-derived radionuclides tend to enter the Arctic Ocean via the Barents Opening.
- The Beaufort Gyre region displays one of the most significant changes in the Arctic Ocean. Both scenarios show a strong increasing trend in flux strength, suggesting an enhanced accumulation of reprocessing-derived radionuclides in the Beaufort Gyre under warmer conditions. However, the radionuclides in the boundary currents of the Beaufort Gyre have longer transit time and deeper depth, suggesting the stronger convection processes; whereas the radionuclides in central waters of the Beaufort Gyre show littler change in transit time and decrease in the depth, suggesting weakened vertical mixing under warmer conditions.
- In the central Nordic Seas, both scenarios show a decreasing trend in flux strength and slight increasing trend in transit time, indicating a reduction in the amount of reprocessing-derived radionuclides entering this region and an enhanced recirculation of radionuclides in this region.

Based on the differences between the SSP245 and SSP585 scenarios shown in **Figures 12C, F, and I** and **Figures 13C, F, and I**, the notable differences of I-129 transport can only be observed in the flux strength of reprocessing-derived radionuclides inside the Arctic Ocean. Compared with the SSP245 scenario, the SSP585 scenario exhibits a weaker flux in the coastal regions of the Barents and Kara Seas (5-15%), the Transpolar Drift Stream (5-25%), and the boundary currents of the Beaufort Gyre (15-25%) and an enhanced flux (15-25%) in the central waters of the Beaufort Gyre, probably due to the change of circulation pattern in the Arctic Ocean. **However, no significant differences can be observed in the Nordic Seas between different climate-warming scenarios within the studied period.**

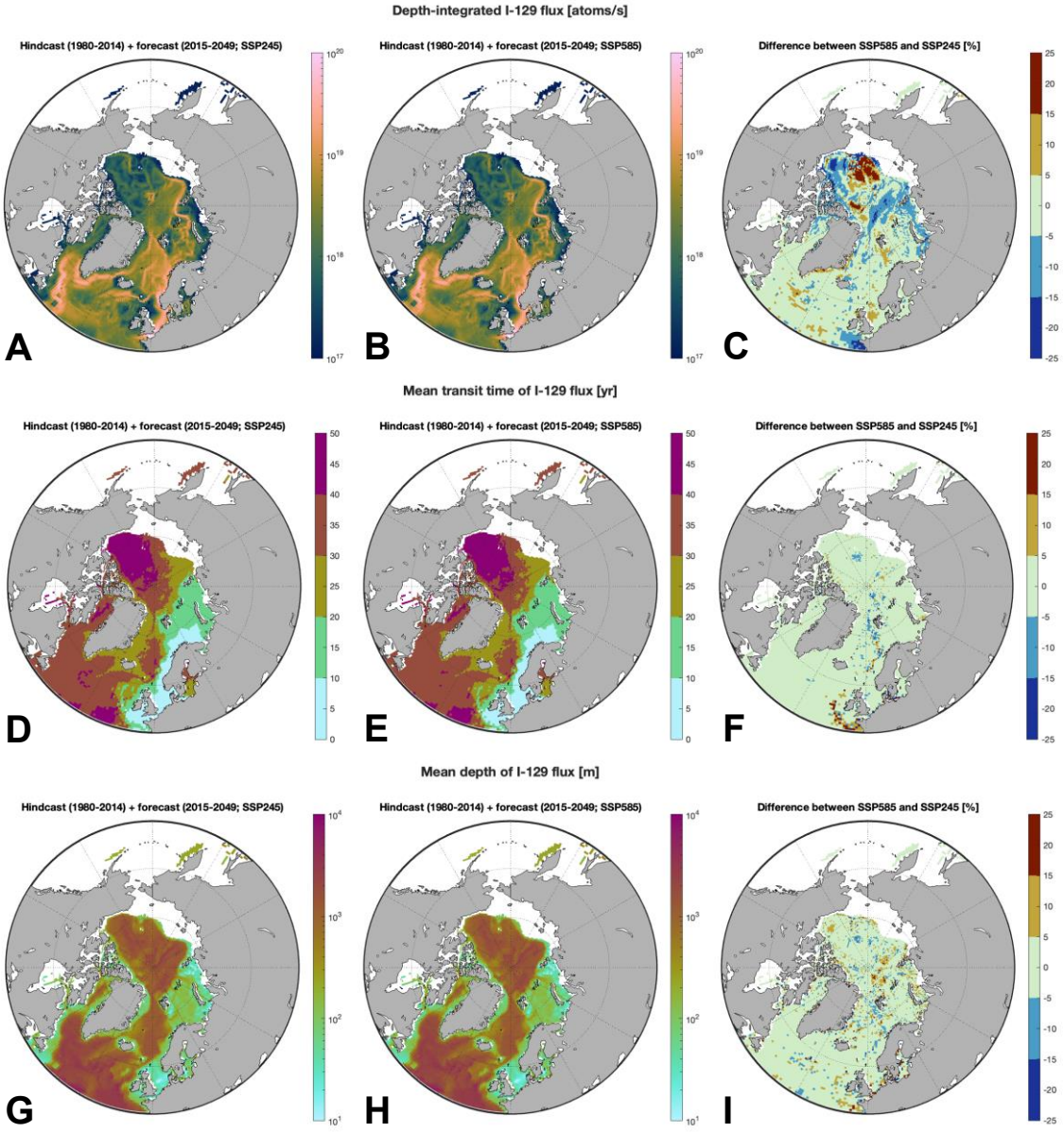

Figure 12. The mean fields for the depth-integrated flux of LH-derived I-129 (atoms/s) (**A** and **B**), the corresponding mean transit time (yr) (**D** and **E**), and the corresponding mean depth (m) (**G** and **H**) for two scenarios: (1) hindcast (1980-2014) + forecast (2015-2049; SSP245); and (2) hindcast (1980-2014) + forecast (2015-2049; SSP585). The differences (%) between the mean fields of the two scenarios are shown in plots **C**, **F**, and **I**.

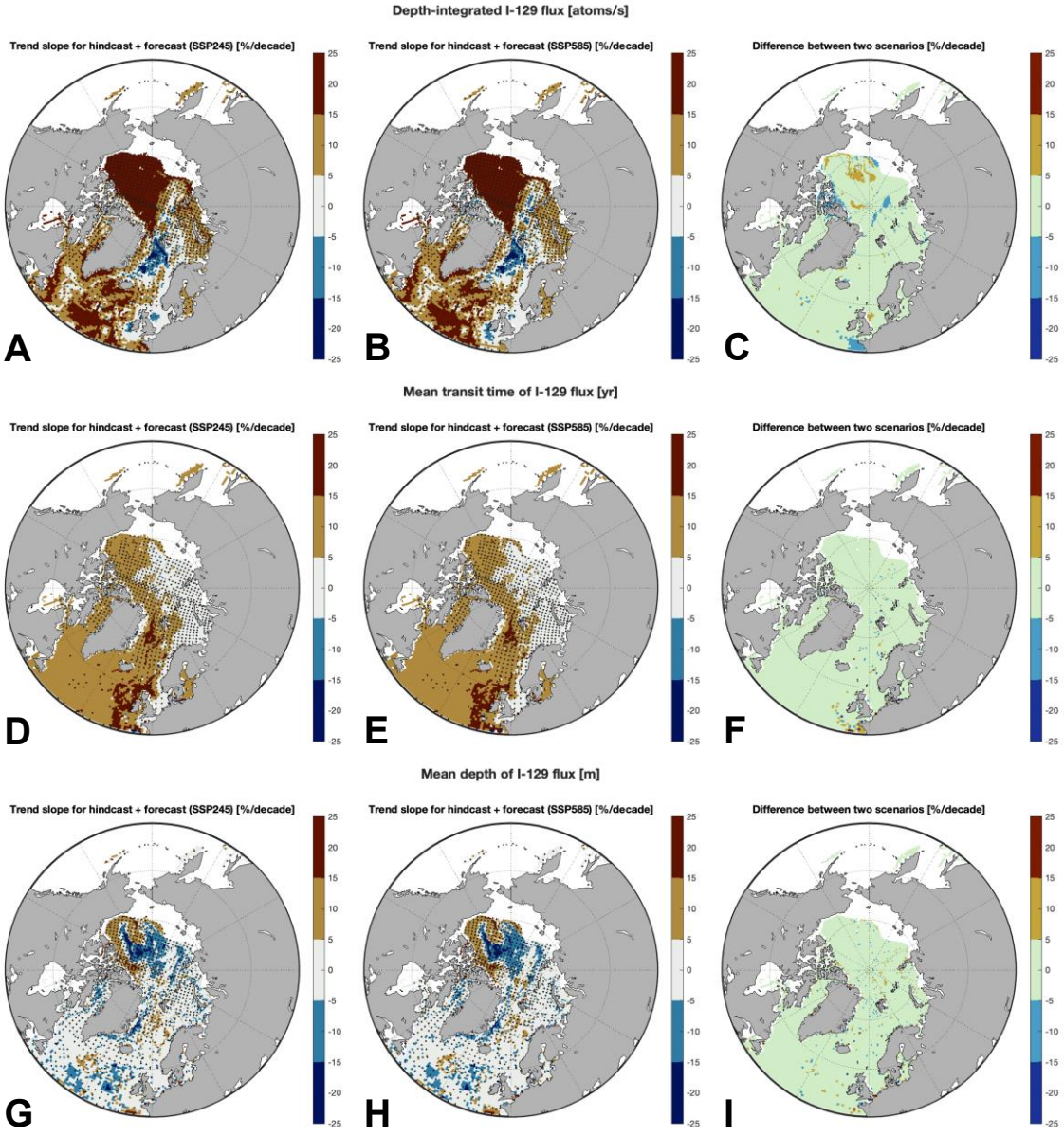

Figure 13. The trend slope (1980-2049) for the depth-integrated flux of LH-derived I-129 (atoms/s) (**A** and **B**), the corresponding mean transit time (yr) (**D** and **E**), and the corresponding mean depth (m) (**G** and **H**) for two scenarios: (1) hindcast (1980-2014) + forecast (2015-2049; SSP245); and (2) hindcast (1980-2014) + forecast (2015-2049; SSP585). The differences (%) between the trend slope fields of the two scenarios are shown in plots **C**, **F**, and **I**. At each grid cell, the trend slope was obtained from the Pearson's Linear Correlation and the black dot represent the trend is significant (p-value < 0.05).

3.2.1.2 Transfer factors in surface waters

The transfer factors of LH-derived radionuclides in surface waters provide valuable insights into the distribution of these radioactive pollutants and the potential radioecological impacts on in the subpolar and polar regions. **Figure 14** presents the mean fields of the transfer factors and transit times of LH-derived radionuclides in the surface waters of the study area. For both climate-warming scenarios, the highest transfer factors (10^2~10^3) are observed in the coastal regions of Western Europe, particularly in the North Sea and along the Norwegian coast. This is expected given the proximity to the release point at La Hague. The transfer factors (**Figure 14A and B**) gradually decrease as they move northward into the Baltic Sea, Arctic Ocean, and Nordic Seas (10~10^2), reflecting the dilution and dispersion of the radionuclides over larger areas. The mean transit times associated with these transfer factors (**Figure 14D and E**) show a clear increasing trend from the source region towards the Baltic Sea, Arctic Ocean, and the Nordic Seas.

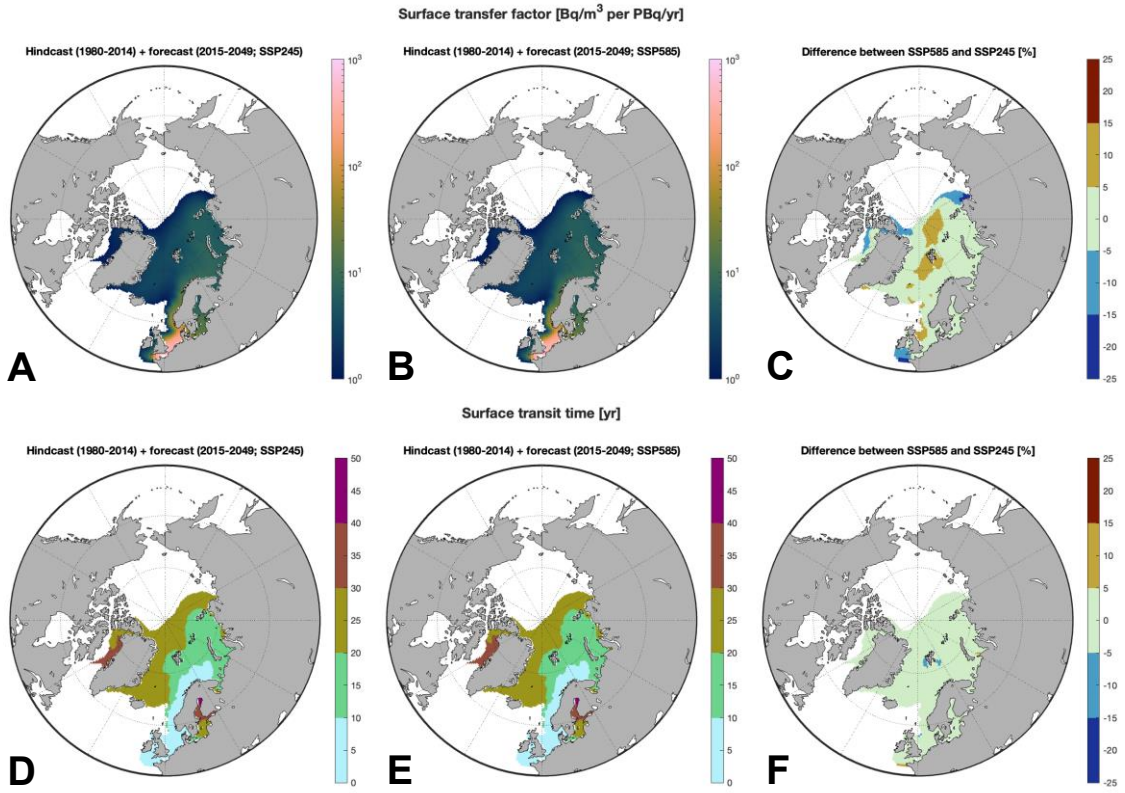

Figure 14. The mean fields for the transfer factors of LH-derived radionuclides (Bq/m3 per PBq/yr) (**A** and **B**) and the corresponding mean transit time (yr) (**D** and **E**) for two scenarios: (1) hindcast (1980-2014) + forecast (2015-2049; SSP245); and (2) hindcast (1980-2014) + forecast (2015-2049; SSP585). The differences (%) between the mean fields of the two scenarios are shown in plots **C** and **F**.

Figure 15 presents the trend slopes for the transfer factors and transit times over the period 1980-2049. **For both climate-warming scenarios, there are no significant changes in the transfer factors and transit times along the major transport pathways of LH-derived radionuclides in the Nordic Seas.**

The only two exceptions are the central Baltic Sea and central Nordic Seas. In the central Baltic Sea, both scenarios show an increasing trend in the transfer factors and transit times, suggesting an accumulation of reprocessing-derived radionuclides in the Baltic Sea over seven decades. Whereas in the central Nordic Seas, both scenarios show an increasing trend in the transit times with no significant changes in the transfer factors, suggesting the recirculation of reprocessing-derived radionuclides in the Nordic Seas.

The differences between the SSP245 and SSP585 scenarios are shown in **Figures 14C and F** and **Figures 15C and F**. **No significant differences can be observed in the Nordic Seas between different climate-warming scenarios within the studied period.** The only exception is the surface waters around Svalbard, where the transfer factors in the SSP585 scenario are slightly higher than those in the SSP245 scenario.

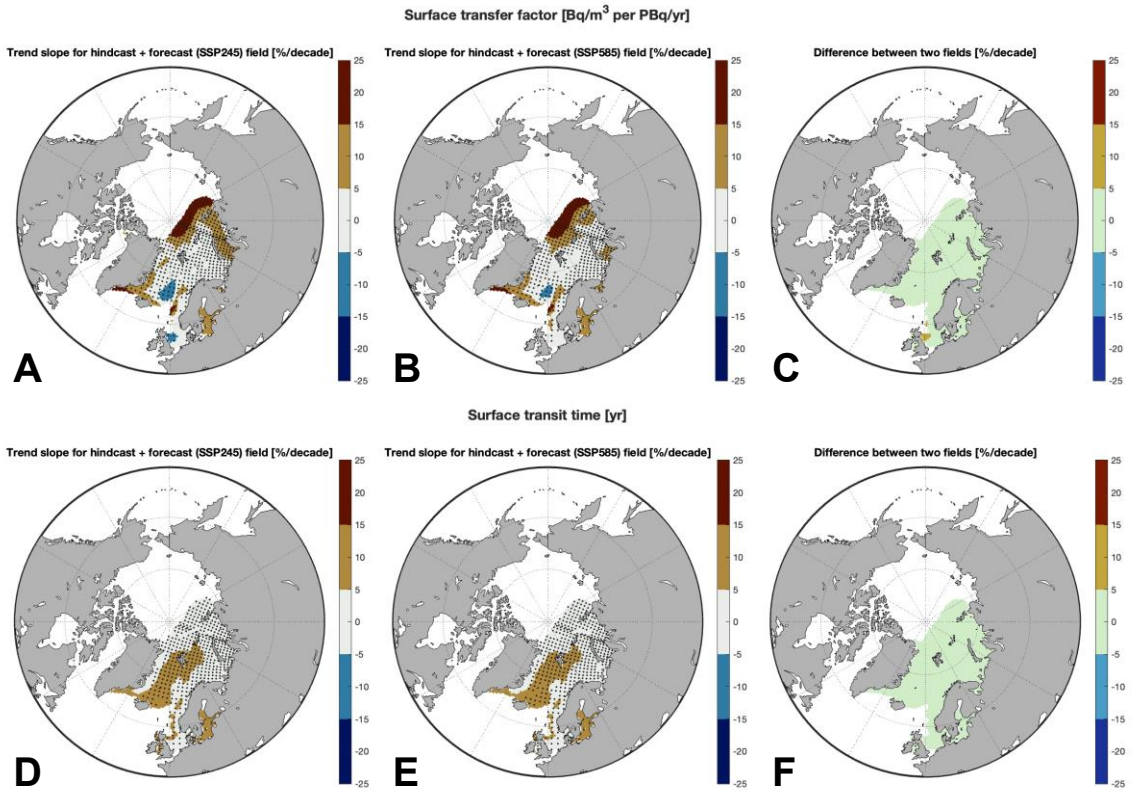

Figure 15. The trend slope for the transfer factors of LH-derived radionuclides (Bq/m3 per PBq/yr) (**A** and **B**) and the corresponding mean transit time (yr) (**D** and **E**) for two scenarios: (1) hindcast (1980-2014) + forecast (2015-2049; SSP245); and (2) hindcast (1980-2014) + forecast (2015-2049; SSP585). The differences (%) between the trend slope fields of the two scenarios are shown in plots **C** and **F**. At each grid cell, the trend slope was obtained from the Pearson's Linear Correlation and the black dot represent the trend is significant (p-value < 0.05).

3.2.2 Accidental releases

To assess the potential impact of a nuclear accident under different climate-warming scenarios, we simulated a hypothetical Fukushima-type accident at the Ringhals Nuclear Power Plant, Sweden. **Figures 16** illustrate the distribution of Cs-137 in surface waters over time for both SSP245 and SSP585 scenarios.

One month after the accident (**Figure 16, A and B**), the initial plume of Cs-137 is concentrated in the Skagerrak and Southwest Norwegian coast, with high concentrations (1000-10000 Bq/kg) observed near the release point. The plume begins to spread northward along the Norwegian coast and southward into the Baltic Sea. By two years post-accident (**Figure 16, D and E**), the plume has significantly dispersed. Elevated concentrations (100-1000 Bq/kg) are observed throughout the Baltic Sea, along the Norwegian coast, and into the Barents Sea. The plume has also begun to enter the Arctic Ocean via the Fram Strait. Five years after the accident (**Figure 16, G and H**), the Cs-137 has spread further into the Arctic Ocean and is detectable in the East Greenland Current. Concentrations in the Baltic Sea and along the Norwegian coast have decreased due to dilution and radioactive decay. Nine years post-accident (**Figure 16, J and K**), the Cs-137 signal is widely distributed across the Arctic Ocean and the Nordic Seas, with concentrations generally below 10 Bq/kg in most areas.

In the Baltic Sea, Cs-137 concentrations remain elevated throughout the simulation period due to the semi-enclosed nature of the basin. Initial concentrations exceed 10 Bq/kg, declining to 1-5 Bq/kg after nine years. In the Nordic Seas, concentrations are highest along the Norwegian coast in the first two years (1-10 Bq/kg) but decrease more rapidly than in the Baltic Sea due to greater water exchange with the North Atlantic. By nine years post-accident, concentrations in the Nordic Seas are generally below 1 Bq/kg. The Arctic Ocean shows a gradual increase in Cs-137 concentrations over time as the plume spreads northward. By the fifth year, concentrations of 0.1-1 Bq/kg are observed across much of the Arctic basin.

The differences between SSP245 and SSP585 scenarios are shown in **Figure 16 C, F, I, and L** for surface concentrations, and in **Figure 14 C, F, I, and L** for inventories. In the first month, differences are minimal, with higher Cs-137 concentrations (>100%) in the vicinity of the accident under the SSP585 scenario. By the second year, more significant differences emerge. The SSP585 scenario shows lower Cs-137 concentrations (20-60%) along the Norwegian coast and in the southern Barents Sea and higher Cs-137 concentrations (>100%) in the northern Barents Sea and western Fram Strait. After five years, the differences become more pronounced. Persistently lower Cs-137 concentrations (20-60%) in the central Baltic Sea and significantly higher Cs-137 concentrations (>100%) in the central Nordic Seas can be observed under SSP585 scenario. By nine years post-accident, the SSP585 scenario shows continued lower Cs-137 concentrations (20-60%) in the Baltic Sea and higher Cs-137 concentrations (> 100%) in the central Nordic Seas and European Arctic. In addition, higher Cs-137 concentrations (> 60%) in the central Arctic Ocean and lower Cs-137 concentrations (20-60%) in the Transpolar Drift Stream can be observed.

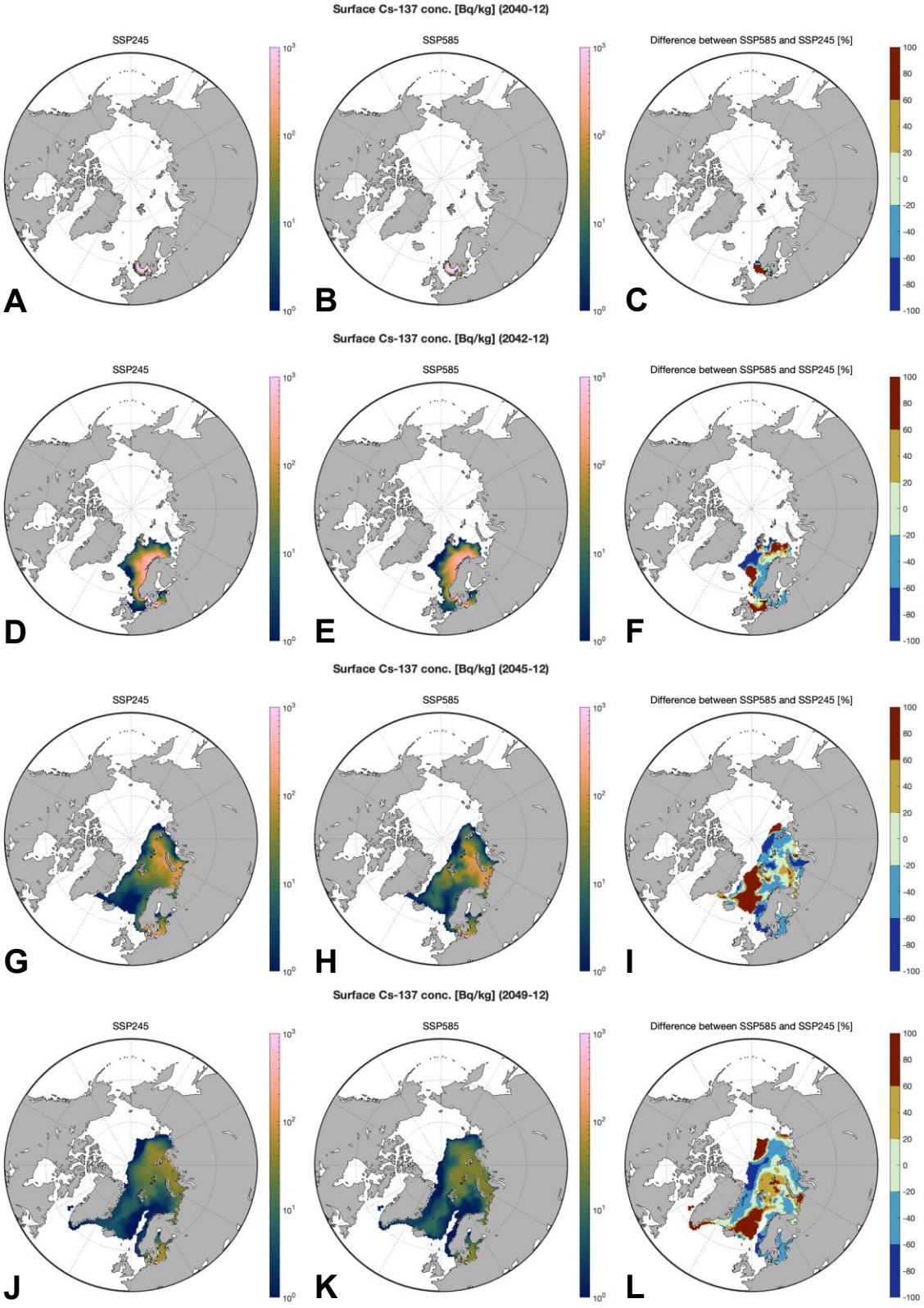

Figure 16. The distribution for the concentration of Cs-137 (Bq/kg) released by a hypothetical nuclear accident in the surface water of the subpolar and Arctic regions 1 month (**A** and **B**), 2 years (**D** and **E**), 5 years (**G** and **H**), and 9 years (**J** and **K**) after the accident for two scenarios SSP245 and SSP585. The differences (%) between the two scenarios are shown in plots **C**, **F**, **I**, and **L**.

3.3 Summary

The projection simulations for 2015-2049 under two climate-warming scenarios (SSP245 and SSP585) revealed several important findings about the future transport of radionuclides in the Nordic Seas and Arctic Ocean:

For authorized discharges from reprocessing plants:

1. Both scenarios showed largely steady-state transport along major pathways entering and exiting the Arctic Ocean. However, notable changes were observed in specific regions:
    - Increased flux into the Arctic Ocean via the Barents Opening
    - Enhanced accumulation of radionuclides in the Beaufort Gyre
    - Reduced transport into the central Nordic Seas

2. Transfer factors and transit times of reprocessing-derived radionuclides in surface waters remained relatively stable along major transport pathways, with some exceptions in the Baltic Sea and central Nordic Seas. Few significant differences were observed between the two climate scenarios in the Nordic Seas.

For the hypothetical nuclear accident scenario:

3. Both climate scenarios showed similar overall transport patterns, but with some notable differences:
    - The SSP585 scenario showed faster initial dispersion but lower long-term concentrations along the Norwegian coast
    - Higher concentrations were observed in the central Nordic Seas under SSP585
    - The Baltic Sea showed persistently lower concentrations in the SSP585 scenario

These results suggest that climate change could lead to shifts in the distribution of radionuclides in the Nordic and Arctic marine environment, with potential implications for ecosystem exposure and human activities in these regions. Also note that the internal variability in each of simulation of climate scenario may be larger than the differences of between these two climate scenarios. An ensemble of simulation of the same climate scenarios are thus needed to separate the impacts of internal climate variability and externally forced climate change. However, this is not done given the limited resources in this project and may be subject to further investigation in the future when it is available.

4. Assessment of Associated Radioecological Risks

4.1 Methodology for dose assessment

Regarding the radioecology assessment in the Nordic marine environment, we considered fish ingestion as the main dose contributor. However, conducting a comprehensive dose assessment for fish ingestion requires surveys on the diet habits and fishery supply chains in the Nordic countries, which is beyond the scope of this project. Instead, a dose factor was calculated (**Equation 1**) for the committed effective dose from ingesting per unit of a fish species captured at a fishing region after releasing per unit of a radionuclide:

$$DF_{f,r} = C_r \cdot CF_{f,r} \cdot IDCF_r \qquad \textbf{Equation 1}$$

where

- $DF_{f,r}$ (in the unit of Sv/kg per Bq): the committed effective dose from ingestion of radionuclide r from fish species f;
- C_r (in the unit of Bq/kg per Bq): concentration of radionuclide r in the seawater of a fishing region sometime after the authorized discharges or accidental releases;
- $CF_{f,r}$ (in the unit of Bq/kg per Bq/kg): concentration factor of radionuclide r from the seawater to the meat of fish species f;
- $IDCF_r$ (in units of Sv/Bq): effective dose coefficients for ingestion by adult (Eckerman et al., 2012).

Uniform concentration factors and ingestion dose conversion factors were used due to their large temporal variabilities. Referring to the concentration process and corresponding concentration factor, we only considered the pathway from seawater to fishes, and the pathway from seawater to sediment and then to fishes was ignored. The dose factors in different climate-warming scenarios were estimated and compared in the major Nordic fishing regions, such as the Norwegian coast, Icelandic coast, and Greenlandic coast, to assess the impacts of climate change on the radioecological safety in the Nordic Seas. Based on the dose factors, decision-makers can easily estimate the dose contribution to the Nordic residents from the consumption of fish products from the Nordic marine environment and take necessary actions if required.

Table 5. The concentration factors and effective dose coefficient selected in the calculation.

	I-129	**Cs-137**	**Sr-90**	**Cs-134**
Concentration factor (L/kg)				
Fish (IAEA)	10 [a]	84 ± 120 [b]	25 ± 39 [b]	same as Cs-137
Effective dose coefficient (adult, Sv/Bq)				
Ingestion [c]	1.1E-07	1.3E-08	2.8E-08	1.9E-08

a (IAEA, 2004)
b (Beresford and Howard, 2014)
c (Eckerman et al., 2012)

4.2 Accidental releases

4.2.1 Effective Doses from Multiple Radionuclides

Figure 17 presents the temporal evolution of effective doses (Sv/kg) at eight stations around the Nordic Seas after a hypothetical nuclear accident under SSP245 scenario. By consuming the fish captured at these stations, the estimated effective doses range from approximately 10^{-7} to 10^{-2} Sv/kg across different stations. Assuming a high fish consumption rate of 100 kg per year, the estimated annual doses will be at the level of 10^{-3} to 10^{-1} Sv by consuming the fish captured at the Danish Straits, Norwegian coastal areas, and the Fram Strait, which are higher or close to the dose limit of 1 mSv (10^{-3} Sv) for public exposure recommended by the International Commission on Radiological Protection (ICRP). Whereas the estimated annual doses will be at the level of 10^{-4} Sv at the Greenlandic and Icelandic coastal areas, which are slightly lower than the recommended dose limit. **Hence, the corresponding countermeasures may be needed for the fishery activities in the Danish, Swedish, and Norwegian waters after the accident.**

At all stations, cesium isotopes (Cs-137 and Cs-134) are the dominant contributors to the effective dose. In the early stages following the accident, particularly within the first 1-2 years, Cs-134 plays a significant role at the Norwegian coastal stations, matching or exceeding the contribution from Cs-137. This is attributed to its higher effective dose coefficient, despite its shorter half-life. As time progresses, the contribution from Cs-134 decreases rapidly due to radioactive decay, and Cs-137 emerges as the predominant dose contributor for the remainder of the simulation period. In contrast, the contributions from I-129 and Sr-90 remain consistently lower than those of the cesium isotopes, typically by one to two orders of magnitude.

4.2.2 Climate-induced Changes in Effective Doses

Figure 18 presents the comparison of estimated effective doses from Cs-137 between the SSP245 and SSP585 scenarios. Shortly after the accident, the SSP585 scenario shows higher effective doses in the vicinity of the accident site, particularly around SW Norwegian Coast. As time progresses, the differences between the two scenarios become more pronounced and geographically diverse. Since the second year after the accident, the SSP585 scenario exhibits lower estimated effective doses along the Norwegian coast (20%~60%), in the Baltic Sea (20%~60%), and the Transpolar Drift (>60%), but higher doses in the central Nordic Seas(>60%). This pattern should be attribute to the shift in the dominant transport pathways under different climate conditions. Overall, the results underscore the importance of considering climate change scenarios in long-term radioecological risk assessments and emergency preparedness planning for the Nordic and Arctic regions.

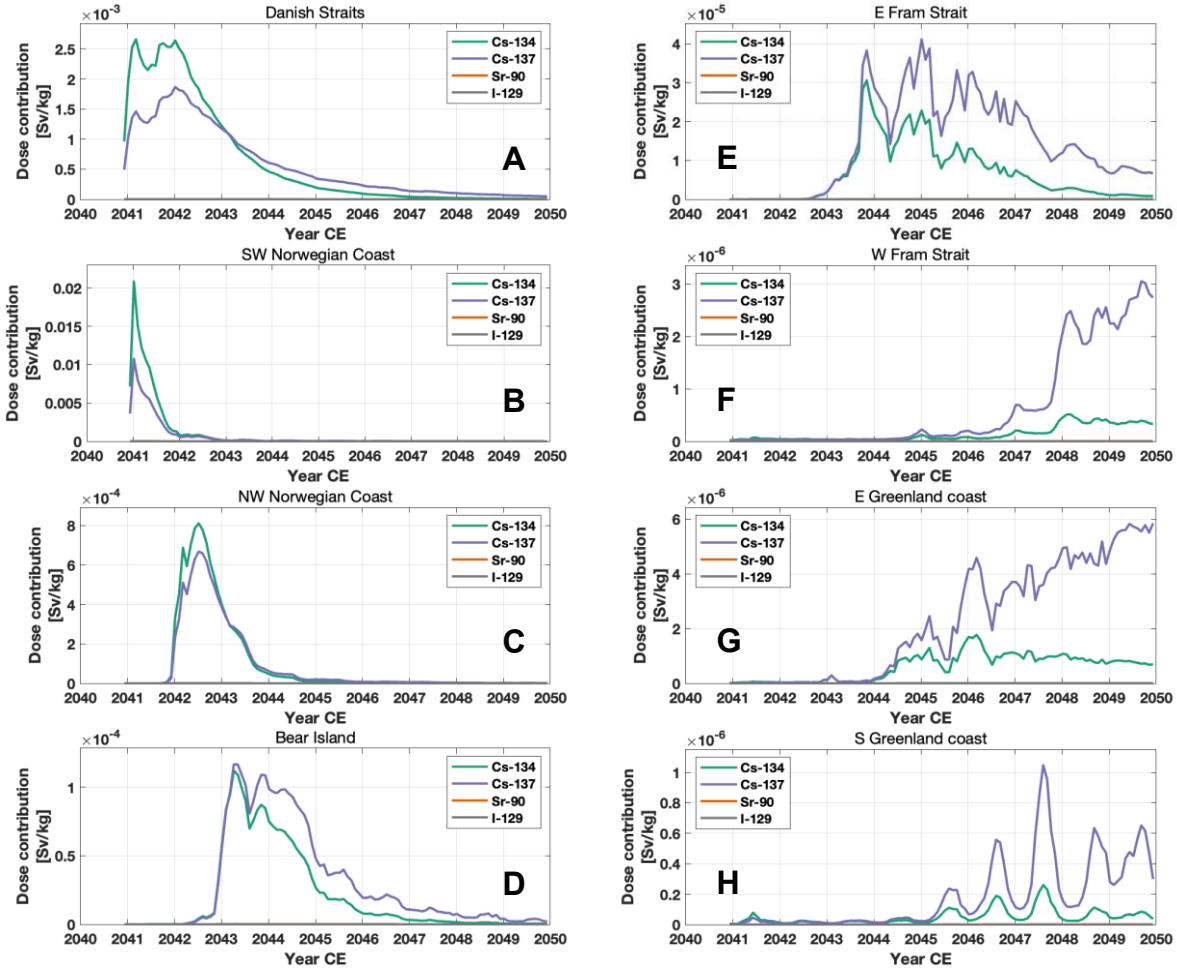

Figure 17. The temporal evolution of estimated effective doses (Sv/kg) of four radionuclides by fish ingestion at eight stations around the Nordic Seas after a hypothetical nuclear accident under SSP245 scenario.

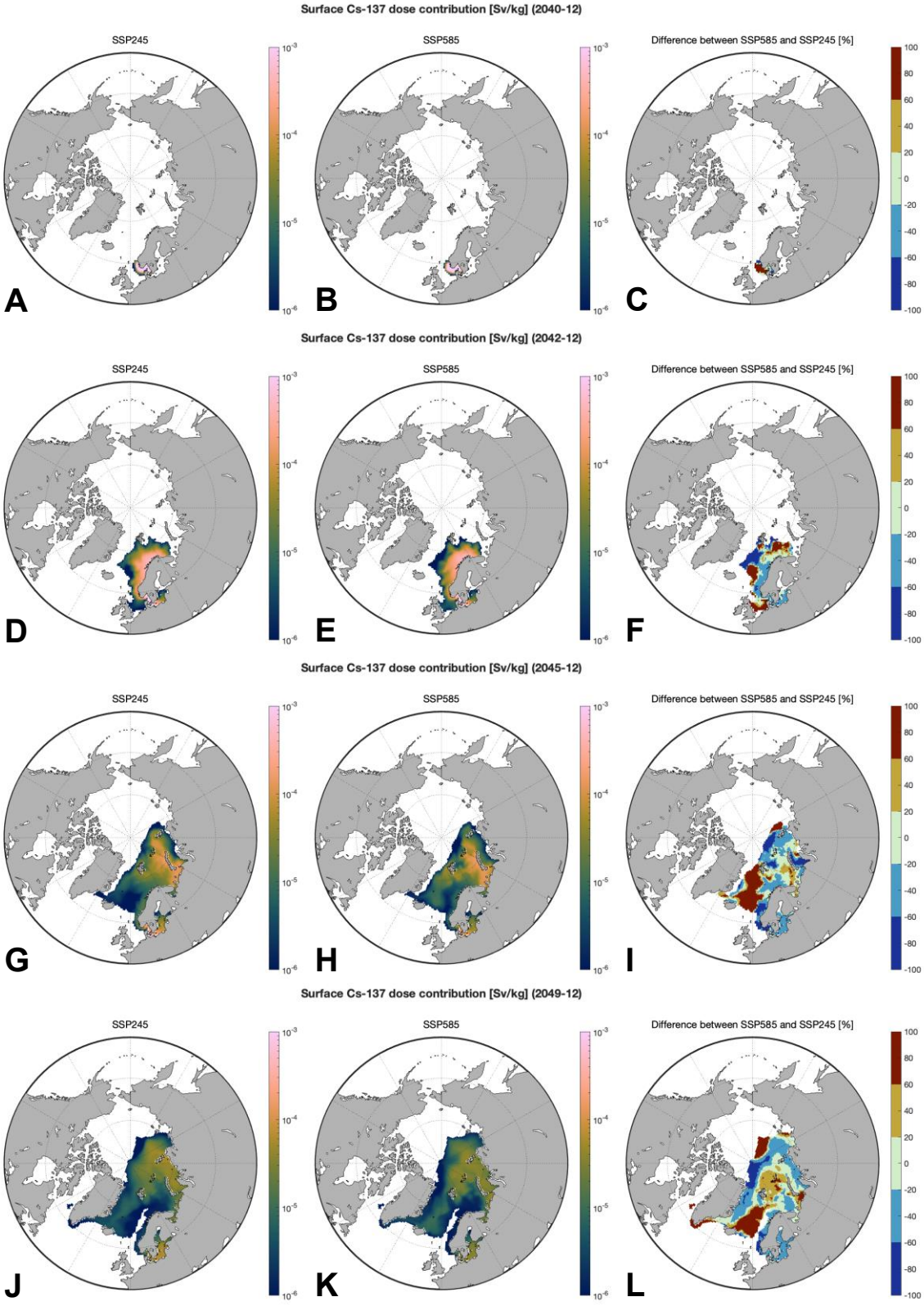

Figure 18. The estimated effective dose of Cs-137 (Sv/kg) by fish ingestion in a hypothetical nuclear accident 1 month (**A** and **B**), 2 years (**D** and **E**), 5 years (**G** and **H**), and 9 years (**J** and **K**) after the accident for two scenarios SSP245 and SSP585. The differences (%) between the two scenarios are shown in plots **C**, **F**, **I**, and **L**.

4.3 Authorized discharges

Figure 19 presents the mean estimated effective doses from LH-derived Cs-137 by fish ingestion for the SSP245 and SSP585 scenarios during 2015-2049. For both scenarios, besides the North Sea, the highest estimated effective doses are observed along the Norwegian coastal waters and in the Baltic Sea (10^{-11} to 10^{-10} Sv/kg per TBq/yr). In the Arctic Ocean and Greenlandic coastal areas, the estimated effective doses further decrease to about 10^{-12} to 10^{-11} Sv/kg per TBq/yr. Even if considering a high fish consumption rate of 100 kg per year, the corresponding estimated annual doses are much lower than the dose limit of 1 mSv (10^{-3} Sv) for public exposure, which have negligible influence from the perspective of radioecological safety.

The comparison between the SSP245 and SSP585 scenarios reveals few differences in the spatial distribution of effective doses. Regarding the dispersion of radioactive discharges from the reprocessing plants, the climate-induced changes can be ignored. **This suggests that current discharge practices may remain acceptable from a dose perspective under near-term climate change scenarios.**

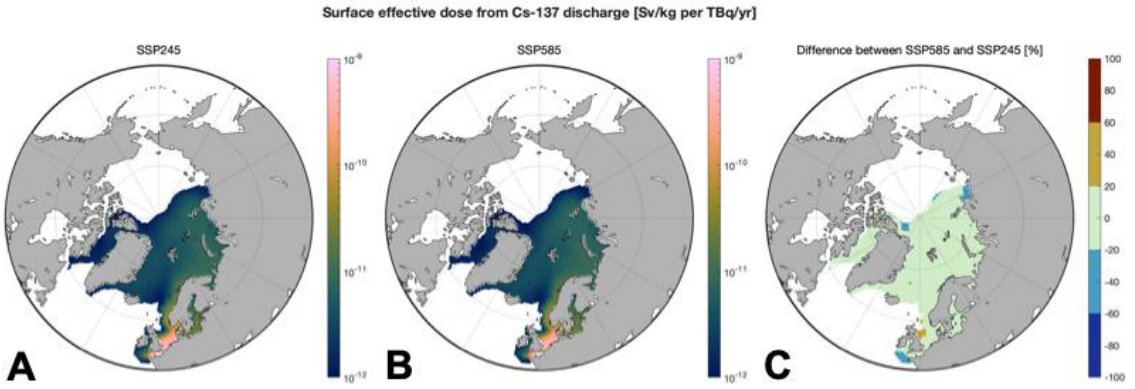

Figure 19. The mean fields for the estimated effective doses of LH-derived Cs-137 (Sv/kg per TBq/yr) (**A** and **B**) by fish ingestion for SSP245 and SSP585 scenarios. The differences (%) between the mean fields of the two scenarios are shown in plot **C**.

4.4 Summary

The assessment of radioecological risks associated with both authorized discharges and accidental releases in the Nordic marine environment revealed the following findings:

- For authorized discharges from reprocessing plants, the estimated effective doses from Cs-137 by fish ingestion are found to be well below the public exposure limit of 1 mSv per year, and the climate-induced changes in the dispersion of these discharges were minimal. These findings suggest that current discharge practices are likely to remain acceptable from a radiological protection standpoint under near-term climate change scenarios.

- For accidental releases from hypothetical Fukushima-type accident: (1) the cesium isotopes are the dominate contributors to the effective doses via fish ingestion, but Cs-134 have less long-term impacts than Cs-137 due to its shorter half-lives; (2) the assessment revealed potentially significant radiological impacts in in the Danish, Swedish, and Norwegian waters, and countermeasures may be needed for the fishery activities after the accident; (3) The SSP585 scenario present higher estimated effective doses in the central Nordic Seas but lower doses in along the Norwegian coastal areas and in the Baltic Sea.

5. References

AMAP, 2016. AMAP Assessment 2015: Radioactivity in the Arctic. Arctic Monitoring and Assessment Programme (AMAP).

Anna Nalbandyan, Inger Margrethe H. Eikelmann, Øyvind Gjølme Selnæs, Øyvind Aas-Hansen, Helmuth Zika, Michael Wallin, Kjartan Guðnason, Jeppe Vöge Jensen, 2017. Scenarios and table top exercise concept on events related to traffic of nuclear-powered vessels and transportation of spent nuclear fuel along the Nordic coastline (COASTEX): Final report (No. NKS-392), Nordic Nuclear Safety Reseach.

Beresford, N., Howard, B., 2014. Handbook of parameter values for the prediction of radionuclide transfer to wildlife. International Atomic Energy Agency.

Bullister, J.L., 2015. Atmospheric histories (1765-2015) for cfc-11, cfc-12, cfc-113, ccl4, sf6 and n2o. Carbon Dioxide Inf. Anal. Cent. Oak Ridge Natl. Lab. US Dep. Energy Oak Ridge Tenn.

Casacuberta, N., Christl, M., Vockenhuber, C., Wefing, A.-M., Wacker, L., Masqué, P., Synal, H.-A., Rutgers van der Loeff, M., 2018. Tracing the Three Atlantic Branches Entering the Arctic Ocean With 129I and 236U. J. Geophys. Res. Oceans 123, 6909–6921. https://doi.org/10.1029/2018JC014168

Casacuberta, N., Masqué, P., Henderson, G., Rutgers van-der-Loeff, M., Bauch, D., Vockenhuber, C., Daraoui, A., Walther, C., Synal, H.-A., Christl, M., 2016. First 236U data from the Arctic Ocean and use of 236U/238U and 129I/236U as a new dual tracer. Earth Planet. Sci. Lett. 440, 127–134. https://doi.org/10.1016/j.epsl.2016.02.020

Casacuberta, N., Smith, J.N., 2023. Nuclear Reprocessing Tracers Illuminate Flow Features and Connectivity Between the Arctic and Subpolar North Atlantic Oceans. Annu. Rev. Mar. Sci. 15, null. https://doi.org/10.1146/annurev-marine-032122-112413

Castrillejo, M., Casacuberta, N., Christl, M., Vockenhuber, C., Synal, H.-A., García-Ibáñez, M.I., Lherminier, P., Sarthou, G., Garcia-Orellana, J., Masqué, P., 2018. Tracing water masses with 129I and 236U in the subpolar North Atlantic along the GEOTRACES GA01 section. Biogeosciences 15, 5545–5564. https://doi.org/10.5194/bg-15-5545-2018

Christl, M., Casacuberta, N., Lachner, J., Maxeiner, S., Vockenhuber, C., Synal, H.-A., Goroncy, I., Herrmann, J., Daraoui, A., Walther, C., Michel, R., 2015. Status of 236U analyses at ETH Zurich and the distribution of 236U and 129I in the North Sea in 2009. Nucl. Instrum. Methods Phys. Res. Sect. B Beam Interact. Mater. At. 361, 510–516. https://doi.org/10.1016/j.nimb.2015.01.005

Eckerman, K., Harrison, J., Menzel, H.-G., Clement, C.H., 2012. ICRP Publication 119: Compendium of Dose Coefficients based on ICRP Publication 60. Ann. ICRP, ICRP PUBLICATION 119: 41, 1–130. https://doi.org/10.1016/j.icrp.2012.06.038

European Commission, 2022. European Commission RAdioactive Discharges Database [WWW Document]. URL https://europa.eu/radd/index.dox

Gidden, M.J., Riahi, K., Smith, S.J., Fujimori, S., Luderer, G., Kriegler, E., van Vuuren, D.P., van den Berg, M., Feng, L., Klein, D., Calvin, K., Doelman, J.C., Frank, S., Fricko, O., Harmsen, M., Hasegawa, T., Havlik, P., Hilaire, J., Hoesly, R., Horing, J., Popp, A., Stehfest, E., Takahashi, K., 2019. Global emissions pathways under different socioeconomic scenarios for use in CMIP6: a dataset of harmonized emissions trajectories through the end of the century. Geosci. Model Dev. 12, 1443–1475. https://doi.org/10.5194/gmd-12-1443-2019

Gómez-Guzmán, J.M., Holm, E., Niagolova, N., López-Gutiérrez, J.M., Pinto-Gómez, A.R., Abril, J.A., García-León, M., 2014. Influence of releases of 129I and 137Cs from European reprocessing facilities in Fucus vesiculosus and seawater from the Kattegat and Skagerrak areas. Chemosphere 108, 76–84. https://doi.org/10.1016/j.chemosphere.2014.03.018

Gómez-Guzmán, J.M., Villa, M., Le Moigne, F., López-Gutiérrez, J.M., García-León, M., 2013. AMS measurements of 129I in seawater around Iceland and the Irminger Sea. Proc. Twelfth Int. Conf. Accel. Mass Spectrom. Wellingt. N. Z. 20-25 March 2011 294, 547–551. https://doi.org/10.1016/j.nimb.2012.07.045

He, P., Pang, H., Yang, Z., Li, S., Huang, Y., Hou, X., Possnert, G., Zheng, X., Pei, X., Aldahan, A., 2022. 127I and 129I species in the English Channel and its adjacent areas: Uncovering impact on the isotopes marine pathways. Water Res. 225, 119178. https://doi.org/10.1016/j.watres.2022.119178

HELCOM, 2020. HELCOM MORS Discharge database [WWW Document]. URL https://helcom.fi/%20baltic-sea-trends/data-maps/databases/ (accessed 5.1.20).

HELCOM, 2018. HELCOM Thematic assessment of radioactive substances in the Baltic Sea 2011–2015 (No. BSEP151).

Hou, X., Aldahan, A., Nielsen, S.P., Possnert, G., Nies, H., Hedfors, J., 2007. Speciation of 129I and 127I in Seawater and Implications for Sources and Transport Pathways in the North Sea. Environ. Sci. Technol. 41, 5993–5999. https://doi.org/10.1021/es070575x

Hou, X., Dahlgaard, H., Nielsen, S.P., 2000. Iodine-129 Time Series in Danish, Norwegian and Northwest Greenland Coast and the Baltic Sea by Seaweed. Estuar. Coast. Shelf Sci. 51, 571–584. https://doi.org/10.1006/ecss.2000.0698

IAEA, 2023. Marine Radioactivity Information System [WWW Document]. URL https://maris.iaea.org/home (accessed 4.23.23).
IAEA, 2004. Sediment Distribution Coefficients and Concentration Factors for Biota in the Marine Environment, Technical Reports Series. INTERNATIONAL ATOMIC ENERGY AGENCY, Vienna.
Iosjpe, M., Isaksson, M., Joensen, H.P., Lahtinen, J., Logemann, K., Pálsson, S.E., Roos, P., Suolanen, V., 2013. Consequences of severe radioactive releases to Nordic Marine environment (No. NKS-296), Nordic Nuclear Safety Reseach.
Kobayashi, S., Ota, Y., Harada, Y., Ebita, A., Moriya, M., Onoda, H., Onogi, K., Kamahori, H., Kobayashi, C., Endo, H., others, 2015. The JRA-55 reanalysis: General specifications and basic characteristics. J. Meteorol. Soc. Jpn. Ser II 93, 5–48.
Lauvset, S.K., Lange, N., Tanhua, T., Bittig, H.C., Olsen, A., Kozyr, A., Álvarez, M., Becker, S., Brown, P.J., Carter, B.R., Cotrim Da Cunha, L., Feely, R.A., Van Heuven, S., Hoppema, M., Ishii, M., Jeansson, E., Jutterström, S., Jones, S.D., Karlsen, M.K., Lo Monaco, C., Michaelis, P., Murata, A., Pérez, F.F., Pfeil, B., Schirnick, C., Steinfeldt, R., Suzuki, T., Tilbrook, B., Velo, A., Wanninkhof, R., Woosley, R.J., Key, R.M., 2021. An updated version of the global interior ocean biogeochemical data product, GLODAPv2.2021. Earth Syst. Sci. Data 13, 5565–5589. https://doi.org/10.5194/essd-13-5565-2021
Lin, G., Qiao, J., Steier, P., Danielsen, M., Guðnason, K., Joensen, H.P., Stedmon, C.A., 2022. Tracing Atlantic water transit time in the subarctic and Arctic Atlantic using 99Tc-233U-236U. Sci. Total Environ. 851, 158276. https://doi.org/10.1016/j.scitotenv.2022.158276
Lin, M., She, J., Murawski, J., Hou, X., Qiao, J., 2023. Long-term environmental risks of the Baltic Sea's "memory effect" revealed by ocean modeling and observation of reprocessing-derived radiotracers. J. Hazard. Mater. 443, 130144. https://doi.org/10.1016/j.jhazmat.2022.130144
Masson-Delmotte, V., Pörtner, H.-O., Roberts, D., Zhai, P., 2019. The ocean and cryosphere in a changing climate : a special report of the Intergovernmental Panel on Climate Change. Intergovernmental Panel on Climate Change, [Geneva] :. 2019.
Nagai, H., Kudo, A., Yamagata, T., Kumamoto, Y., Nishino, S., Matsuzaki, H., 2019. The 2013-15 temporal variation in the 129I concentration in seawater in the southern Canada Basin. Nucl. Instrum. Methods Phys. Res. Sect. B Beam Interact. Mater. At. 455, 305–310. https://doi.org/10.1016/j.nimb.2019.01.036
Nalbandyan, A., Aas-Hansen, Ø., Eikelmann, I.M.H., Lindgren, J., Guðnason, K., Peltonen, T., Jensen, J.V., 2016. Nuclear icebreaker traffic and transport of radioactive materials along the Nordic coastline: response systems and cooperation to handle accidents (NORCOP-COAST) (No. NKS-362), Nordic Nuclear Safety Reseach.
Nielsen, S.P., Iosjpe, M., Strand, P., 1995. A preliminary assessment of potential doses to man from radioactive waste dumped in the Arctic Sea.
Nies, H., Goroncy, I., Herrmann, J., Michel, R., Daraoui, A., Gorny, M., Jakob, D., Sachse, R., Tosch, L., Nielsen, S., 2008. Vorhaben StSch 4481: Kartierung von Tc-99, I-129 und I-127 im Oberflächenwasser der Nordsee.
Qiao, J., Hain, K., Steier, P., 2020. First dataset of 236U and 233U around the Greenland coast: A 5-year snapshot (2012–2016). Chemosphere 257, 127185. https://doi.org/10.1016/j.chemosphere.2020.127185
Qiao, J., Zhang, H., Steier, P., Hain, K., Hou, X., Vartti, V.-P., Henderson, G.M., Eriksson, M., Aldahan, A., Possnert, G., Golser, R., 2021. An unknown source of reactor radionuclides in the Baltic Sea revealed by multi-isotope fingerprints. Nat. Commun. 12, 823. https://doi.org/10.1038/s41467-021-21059-w
Reistad, O., Hustveit, S., Pálsson, S.E., Hoe, S., Lahtinen, J., 2012. A Nordic approach to impact assessment of accidents with nuclear-propelled vessels (No. NKS-268), Nordic Nuclear Safety Reseach.
Seland, Ø., Bentsen, M., Olivié, D., Toniazzo, T., Gjermundsen, A., Graff, L.S., Debernard, J.B., Gupta, A.K., He, Y.-C., Kirkevåg, A., Schwinger, J., Tjiputra, J., Aas, K.S., Bethke, I., Fan, Y., Griesfeller, J., Grini, A., Guo, C., Ilicak, M., Karset, I.H.H., Landgren, O., Liakka, J., Moseid, K.O., Nummelin, A., Spensberger, C., Tang, H., Zhang, Z., Heinze, C., Iversen, T., Schulz, M., 2020. Overview of the Norwegian Earth System Model (NorESM2) and key climate response of CMIP6 DECK, historical, and scenario simulations. Geosci. Model Dev. 13, 6165–6200. https://doi.org/10.5194/gmd-13-6165-2020
Sergey Galushin, Anders Riber Marklund, Dmitry Grishchenko, Pavel Kudinov, Tuomo Sevón, Sara Ojalehto, Ilona Lindholm, Patrick Isaksson, Elisabeth Tengborn, Naeem Ul-Syed, 2022. Source Term And Timing Uncertainty in Severe Accidents (No. NKS-461), Nordic Nuclear Safety Reseach.
Smith, J.N., Karcher, M., Casacuberta, N., Williams, W.J., Kenna, T., Smethie Jr., W.M., 2021. A Changing Arctic Ocean: How Measured and Modeled 129I Distributions Indicate Fundamental Shifts in Circulation Between 1994 and 2015. J. Geophys. Res. Oceans 126, e2020JC016740. https://doi.org/10.1029/2020JC016740
Vivo-Vilches, C., López-Gutiérrez, J.M., Periáñez, R., Marcinko, C., Le Moigne, F., McGinnity, P., Peruchena, J.I., Villa-Alfageme, M., 2018. Recent evolution of 129I levels in the Nordic Seas and the North Atlantic Ocean. Sci. Total Environ. 621, 376–386. https://doi.org/10.1016/j.scitotenv.2017.11.268

Wefing, A. -M., Christl, M., Vockenhuber, C., Rutgers van der Loeff, M., Casacuberta, N., 2019. Tracing Atlantic Waters Using 129I and 236U in the Fram Strait in 2016. J. Geophys. Res. Oceans 124, 882–896. https://doi.org/10.1029/2018JC014399

Title	Assessment of climate change's impacts on radioecological safety of subpolar and Nordic marine environment: Final Report from the NKS-B ANTHROPIC
Author(s)	Mu Lin, Jixin Qiao, Sven P. Nielsen, Gang Lin, Yanchun He, Annette Samuelsen, Emil Jeansson, Kjartan Guðnason, Karin Aquilonius, Pål Andersson, Anna Maria Blixt Buhr, Vesa-Pekka Vartti, Pia Keski-Jaskari
Affiliation(s)	Technical University of Denmark (Denmark) Nansen Environmental and Remote Sensing Center (Norway) Norwegian Research Centre (Norway) Icelandic Radiation Safety Authority (Iceland) Swedish Radiation Safety Authority (Sweden) Radiation and Nuclear Safety Authority (Finland)
ISBN	87-7893-7893-584-7
Date	October 2024
Project	NKS-B ANTHROPIC
No. of pages	39
No. of tables	5
No. of illustrations	19
No. of references	37

Abstract
max. 2000 characters

This NKS-B ANTHROPIC project assesses climate-change impacts on radionuclide transport in Nordic and Arctic marine environments and associated radioecological risks using the Norwegian Earth System Model (NorESM).

NorESM was evaluated using historical data of reprocessing-derived radiotracers and chemical tracers, showing good performance, particularly in the Nordic Seas.

We simulated radionuclide transport from authorized discharges and a hypothetical nuclear accident under two different climate scenarios for 2015-2049. For authorized discharges, projections show largely steady-state transport along major pathways, with regional changes including increased flux into the Arctic Ocean via the Barents Sea and enhanced accumulation in the Beaufort Gyre. Few significant differences were observed between climate scenarios in the Nordic Seas. For hypothetical accident, the warmer climate showed lower long-term concentrations along the Norwegian coast, higher

concentrations in central Nordic Seas, and lower concentrations in the Baltic Sea.

Risk assessments indicate that for authorized discharges, estimated doses remain well below public exposure limits with minimal climate-induced changes. For accidental releases, potentially significant impacts were identified in Danish, Swedish, and Norwegian waters, with cesium isotopes dominating dose contributions.

These findings suggest that current authorized discharge practices likely remain acceptable under near-term climate scenarios, but the long-term impacts on the radioecological risk and emergency preparedness needs to be investigated.

Key words Radionuclide transport, Climate change, Nordic marine environment, Earth system model